Doctoral Dissertation

Functionalization of Chitosan-Cellulose Composite Materials Utilizing Cross-Links as Key Structures

架橋を鍵構造として利用したキトサン–セルロース複合材料の機能化

Horathal Pedige Madhurangika Panchabashini

June 2024

Graduate School of Engineering

Osaka University

Table of Contents

General Introduction

Polysaccharides

The December 2009 UN climate change conference underscored the environmental challenges, including global warming wrought by economic globalization, population growth, and human actions often heedless of their ecological consequences. This event catalyzed multi-level discourse across politics, science, and business realms, initiating a historical debate on the imperative of CO_2 neutrality and transitioning to a bio-based economy. Synthetic polymer-based materials such as conventional plastics from fossil fuels greatly impact the environment by choking marine wildlife, damaging the soil, poisoning the groundwater, and polluting the air.[1]

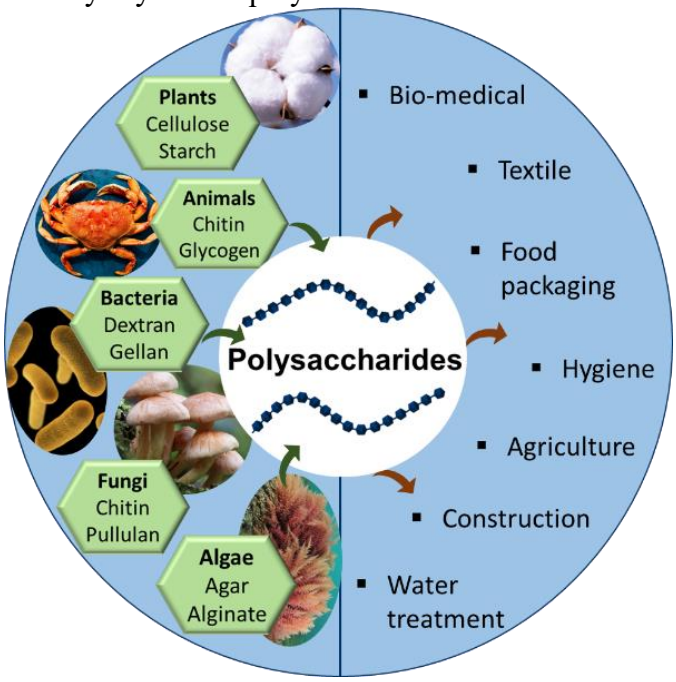

Figure 1. The variety of polysaccharide sources and multiple applications of polysaccharides.

Polysaccharides emerge as linchpins in transitioning to a bio-based economy, offering promising solutions to the world's pressing challenges mainly caused by synthetic polymer-based materials. Polysaccharides are promising substitutes for hazardous materials such as conventional plastics. Foreseen as pivotal to a sustainable future, polysaccharides are poised to revolutionize food production, fuel generation, material construction, and pharmaceutical development

Polysaccharides are Earth's most abundant natural polymers, composed of repeated monomeric sugars linked by glycosidic bonds. They can be differentiated according to the nature of the monosaccharide, the length of chains, and the chain branching.[2] Polysaccharides serve indispensable roles in living organisms' structural integrity, energy metabolism, cell-cell communication, adhesion, and molecular recognition.[3,4]

Polysaccharides are extremely diverse sets of materials that come from various natural sources (**Figure 1**). Plants are the main providers, storing them as energy and using them as structural materials. Starch is the primary storage polysaccharide in plants, while cellulose is the main structural one. Plants also supply pectin and various gums. In animals, polysaccharides have both structural and storage roles. Chitin is the main structural material in crustaceans and some fungi, and glycogen is the energy-storage polysaccharide mainly in mammalians. Hyaluronic acid is found in the tissues and fluids of vertebrates. Some bacteria produce xanthan, dextran, and gellan, while some fungi produce elsinan, pullulan, ß-glucan, and galactans. Because of their wide range of sources and properties like biocompatibility, stability, non-toxicity, and biodegradability, polysaccharides are used in many fields including food, textiles, biomedical applications, hygiene, agriculture, construction, and wastewater treatment.[5,6]

Chitosan (CS)

Chitosan is the deacetylated product of chitin, a widely occurring biopolymer in nature, and can be found in the exoskeletons of a range of eukaryotes such as crustaceans (Crab and Shrimp shells), and insects (cuticle, ovipositors, and cocoons). Some fungi (*Mucor rouxii, Aspergillus nidulans*) and centric diatoms (*Thalassiosira fluviatilis*) also produce chitin. It is the second most abundant polymer in nature following cellulose. Industrial-scale chitin extraction primarily utilizes crustacean shells and fungal mycelia as main sources

Chitin can be deacetylated mainly using alkaline conditions to produce chitosan, a linear polysaccharide comprising randomly distributed D-glucosamine and *N*-acetyl-D-glucosamine units linked by *ß*-(1→4) glycosidic linkages. The distribution of those units varies the molecular chain length, sequence, and composition of chitosan. The mole fraction of the repeating unit with the free amino group is known as the degree of deacetylation (DD), an important parameter in chitosan characterization. The cut-off DD values of chitin to chitosan are around 40-70 % according to different literature. Mostly, commercial chitosan contains a DD of around 70-90 %.[7,8] Chitosan can be set apart from other polysaccharides such as cellulose and chitin due to the subsequent characteristics that are inherited due to the

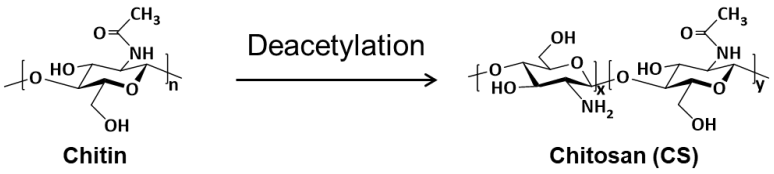

Figure 2. The chemical illustration of chitin and chitosan.

presence of the primary amine group. The 2-amino-2-deoxyglucose units make the polymer soluble in aqueous acidic solutions through the protonation of the amino group, followed by salt formation. As a primary aliphatic amine with a pK_a value of 6.3-6.5, chitosan can be protonated by acids such as acetic acid. It has a prominent capacity to form polyelectrolyte complexes with a variety of synthetic or natural anionic materials due to its cationicity. Also, chitosan is a prominent nitrogen source in various fields such as agriculture.

Apart from the common characteristics of being a polysaccharide, chitosan has important properties such as antioxidant, antibacterial, wound healing acceleration, mucoadhesive, immune system stimulative, analgesic, and hemostatic properties which make it highly advantageous for biomedical applications. Its ability to blend with various materials[9], be processed into two-dimensional and three-dimensional forms, and chelate with metals significantly broadens the scope of chitosan's applications across numerous fields.[10–12] The global chitosan market is substantial, roughly estimated at approximately $7 billion per year. Chitosan-based products meet the requirements of Generally Recognized As Safe (GRAS) which was stipulated by the Food and Drug Administration (FDA), making chitosan a safer material to be used in food, cosmetics, and medical devices worldwide, especially in the USA, Japan, Italy, and Finland.[13,14]

Some notable biomedical applications for chitosan include tissue engineering, wound-healing bandages, and sponge production[15], anti-inflammatory products and tumor-inhibitive drug production, and target drug delivery.[16,17] In the agriculture sector chitosan is used for seed and leaf coating material synthesis, fertilizer production, and time-related drug delivery. In food processing, chitosan is utilized as a material for food storage and food preservation,[18–20], as well as a nutrition enhancer. Chitosan-based three-dimensional materials are extensively used in wastewater treatment to remove hazardous metal ions such as lead, mercury, anionic dyes[21–23], and microplastics.[24] Additionally, chitosan is commonly incorporated as an additive in cosmetics.

Chitosan nanofibers (CSNFs)

Polysaccharide nanofibers are widely recognized for their high aspect ratios and small diameters. Chitosan nanofibers (CSNFs) have recently attracted significant attention as renewable building blocks for creating functional materials as novel green alternatives. These nanofibers exhibit intriguing mechanical, morphological, and optical properties. Multiple fabrication methods exist for chitosan nanofibers, including electrospinning, ultrasonication, grinding, atomization, and

aqueous counter-collision (ACC).[25] Although electrospinning is a common technique for producing nanofibers with controlled scales, it requires high electrical forces when used for chitosan due to the high surface tension from the cationicity of chitosan solutions.[26,27] Furthermore, electrospinning can reduce the mechanical strength of nanofibers because the drastic solvent evaporation scours the fiber surface. On the other hand, the ACC method employs a high-pressure water jet system to efficiently disintegrate chitosan into thinner fibers on a large scale using a ball-collision chamber. This method yields exceptional characteristics, such as fine micro- and nanoscale fibrous structures with extensive specific surface areas and stable high water dispersibility. Additionally, chitosan nanofibers produced this way demonstrate superior properties due to the retention of chitosan's inherent structural integrity post-ACC treatment.[28]

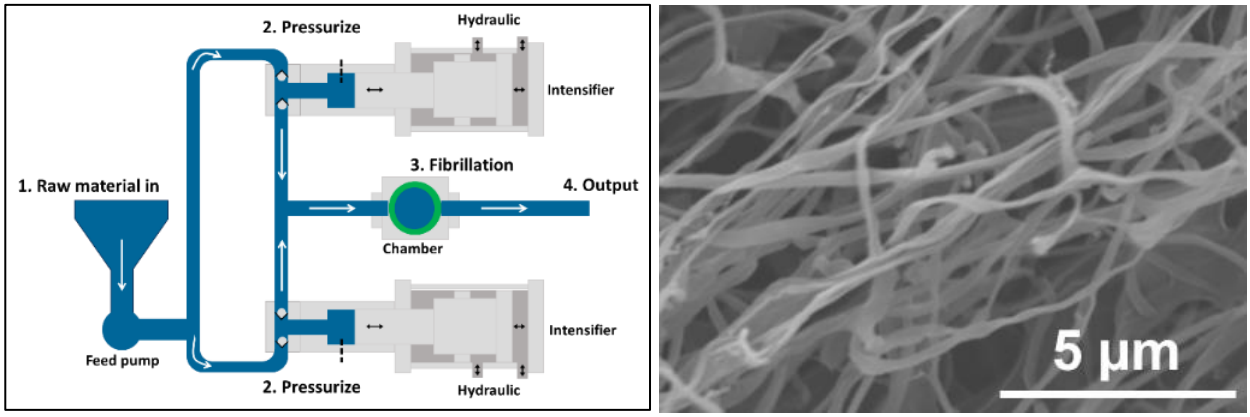

Figure 3. The illustration for the high-pressure water jet system in the fibrillation of chitosan nanofibers[28], and the SEM image of chitosan nanofiber fibrillated using this process.

Cross-linking techniques of chitosan-based materials

Despite being a beneficial polysaccharide utilized in various applications, chitosan suffers from poor mechanical properties, high swellability in aqueous conditions, and low persistence. To address these limitations and produce stable chitosan-based materials, it is essential to perform cross-linking or modification of chitosan. Furthermore, cross-linking chitosan with diverse materials can impart intriguing properties to the composite materials, enhancing their functionality.[29] Chitosan chains have reactive groups including primary amine groups and primary and secondary hydroxyl groups. Cross-linking of chitosan can occur through these reactive groups using both chemical and physical interactions. Multifunctional polymer networks can be created

by blending chitosan with suitable polymers or molecules and utilizing various cross-linking agents.[30]

Imine bonds, also known as Schiff bases, are the most commonly used chemical cross-linking method for chitosan due to the high reactivity of chitosan's primary amine groups with aldehyde groups. Glutaraldehyde was once popular as a dialdehyde cross-linker in early research, but its bio-toxicity has led researchers to favor green and low-toxic materials with aldehyde groups, such as oxidized polysaccharides.[31] Imine bonds can be reduced to secondary amines. In addition to chemical interactions, electrostatic interactions are frequently employed in the physical cross-linking of chitosan. As a cationic polymer, chitosan can electrostatically interact with various anionic materials, including low molecular weight substances like phosphates and polymers like alginate.[32] Additionally, hydrogen bonding between the abundant hydroxyl groups and primary amine groups of chitosan significantly contributes to blending chitosan with other materials and enhancing its properties.[33]

Table No.1: Chitosan cross-linking methods and various cross-linkers.

Cross-linking type	Cross-linker	Application	Reference
Imine bond	oxidized dextran	in-situ gellable hydrogels food packaging	34–36
	oxidized sodium alginate	tissue engineering drug delivery	37–39
	oxidized hyaluronic acid	wound healing	40–42
	oxidized cellulose	hemostasis agents	43,44
Amide bond	poly(ethylene glycol)	wound healing dye removing	45,46
	poly($_L$-glutamic acid)	cartilage regeneration	47

Heterocyclic amine and secondary amine bond	genipin	tissue engineering wound healing	48–50
	diepoxy-poly(ethylene glycol)	cell proliferation	51
Ionic interactions	sodium triphosphate	dye removal food packaging	52–54
	alginate	antibacterial materials cell growing	55,56

Cellulose

Cellulose is one of the most abundant organic materials and polysaccharides on Earth, serving as the primary component of plants. It is an unbranched polymer composed of repeating glucose units $(C_6H_{10}O_5)_n$ linked by β (1→4) bonds. A single cellulose chain comprises both crystalline and amorphous domains, making it a semicrystalline material.[57] Due to the structural rigidity of its polymer chains, cellulose and its derivatives exhibit excellent physicochemical stability, with a lower density and high mechanical properties.[58] Its flexibility, chemical functionality, and ability to blend into various materials are crucial for designing sustainable materials with desired functions.[59,60] Choosing the appropriate form of cellulose and its derivatives is essential based on the intended application. One notable form is cellulose nanofibers (CNFs), which demonstrate excellent mechanical strength due to the sophisticated crystalline structure of cellulose. Cellulose nanofibers have garnered interest as building blocks for bio-based functional materials. Additionally, water-soluble cellulose derivatives hold great potential as structural components for developing bio-based materials, thanks to the easy and safe handling of the polymers and the inherent beneficial characteristics of cellulose. Common examples of cellulose utilization include paper production[61,62], the textile industry[63,64], and biomedical applications[65,66]. Furthermore, cellulose and its derivatives are prime candidates for cross-linkers of chitosan, owing to their designability and modifiability. Chitosan-cellulose blended materials are widely used in various fields, particularly in biomedical applications.

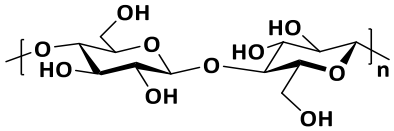

Figure 4. The chemical illustration of cellulose anhydroglucose unit.

Bacterial Cellulose (BC)

BC, also known as microbial cellulose and bacterial nanocellulose, is produced by bacteria and was first discovered by Brown in 1886.[67] It is a natural hydrogel, primarily produced by Gram-negative bacteria such as *Komagataeibacter xylinus*, *Agrobacterium*, *Achromobacter*, *Aerobacter*, *Azotobacter*, *Pseudomonas*, and *Rhizobium*, with *Sarcina* being the only Gram-positive bacteria known to produce bacterial cellulose. Among these, *Komagataeibacter xylinus* is the most commonly used in BC production. A wide range of carbon and nitrogen sources can serve as substrates for cultivating BC-producing bacteria.[68]

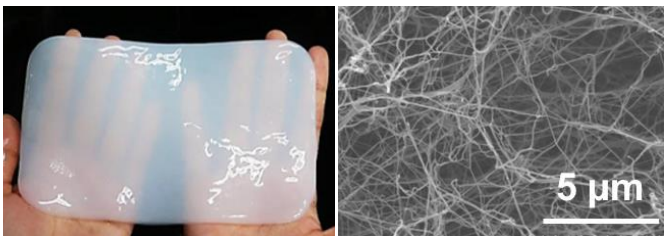

Figure 5. A photograph of a BC hydrogel and the SEM image of the CNFs network structure in BC.

Bacterial cellulose has various morphological forms, including fleece, films, spheres, and hollow particles, which are versatile for designing biomedical materials. It is a highly pure material (>90%) and does not bind to polymers such as hemicellulose and lignin, making its isolation and purification straightforward without extensive chemical treatments. Bacterial cellulose features an ultrafine fiber network with a remarkable crystalline structure. Its intertwined network of cellulose nanofibers (CNFs) with intermolecular and intramolecular hydrogen bonds endows bacterial cellulose with high mechanical strength and good elasticity. Additionally, bacterial cellulose can hold a large amount of water due to its unique nanomorphology, large surface area, and extreme porosity. It is also chemically stable and non-toxic.[69,70]

These exceptional properties make bacterial cellulose suitable for various biomedical applications, including tissue engineering[71], the pharmaceutical industry[72], drug delivery[73–75], wound regeneration, and the immobilization of enzymes and biomolecules.[76] Furthermore, bacterial cellulose is utilized in the paper industry[77] and serves as a stable matrix for synthesizing hydrogel composites with special characteristics like stimuli responsiveness. Bacterial cellulose is an appropriate matrix for chitosan immobilization as a strong and three-dimensionally stable cellulose nanofiber network.

Carboxymethyl cellulose (CMC)

CMC is a type of cellulose ether produced through the partial or complete etherification of cellulose hydroxyl groups. This process involves reacting cellulose with monochloroacetic acid, resulting in cellulose with C2, C3, and C6 hydroxyl groups substituted by carboxymethyl groups.[78] Commercially, carboxymethyl cellulose is available as a sodium salt and is characterized by features such as its poly-anionic nature, high chemical stability, hydrophilicity, and water solubility. However, it is insoluble in organic solvents like ethanol. The water solubility of carboxymethyl cellulose depends on the degree of substitution and the distribution of the substituted groups along the polymer chain.

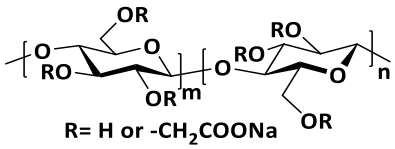

Figure 6. The chemical structure of carboxymethyl cellulose .

carboxymethyl cellulose is utilized in numerous biomedical applications, including tissue engineering, wound dressing, drug delivery, and drug emulsification.[79–82] Additionally, carboxymethyl cellulose serves as a viscosity-increasing agent, binder, stabilizer, and rheological control agent in the food processing, packaging[83], and textile[84] industries. Furthermore, carboxymethyl cellulose is an effective chitosan cross-linking material with multiple cross-linking possibilities.

Cellulose oxidation

Chemical derivatization of pristine cellulose is a robust method to meet the demands of fabricating high-performance materials both chemically and dimensionally. The oxidation can be either selective or non-selective. Selective oxidation of cellulose is a valuable approach to producing high-performance cellulose with versatile applications.[85,86] Common selective oxidation methods include the oxidation of cellulose using TEMPO and sodium periodate. Oxidation of cellulose using sodium periodate is a straightforward oxidation that requires mild reaction conditions.[87] This oxidation occurs by attacking the vicinal hydroxyl groups at C2 and C3, cleaving the C2-C3 bond in the anhydroglucose unit and resulting in vicinal aldehyde groups.[88] Dialdehyde cellulose (DAC) can be further modified through Schiff base formation,

cationization[89], oxidation into dicarboxylic groups[90], reduction into dialcohols[91], silanization[92], and sulfonation[93].

Dialdehyde cellulose is an excellent candidate for cross-linking chitosan networks. The cross-linking primarily occurs through the formation of Schiff bases utilizing the aldehyde groups of DAC and the primary amine groups of chitosan. Additionally, the abundance of hydroxyl groups in both polymers allows for hydrogen bonding, enhancing the stability of the network. Furthermore, using oxidized anionic cellulose like carboxymethyl cellulose (CMC) can form electrostatic interactions, thereby improving the properties of the cellulose-chitosan network.[94–98]

Outline of this thesis

In this doctoral thesis, the author presented the fabrication of chitosan-cellulose composite materials functionalized with multiple cross-linking techniques for different applications. Various methods were employed in the composite fabrication, leveraging the structural and chemical diversity of both chitosan and cellulose. In Chapter 1, stimuli-responsive composite hydrogels were prepared using oxidized cellulose nanofibers (CNFs) and chitosan (CS). Chapter 2 detailed the creation of multifunctional chitosan nanofiber-based sponge materials using chitosan nanofibers (CSNFs) and dialdehyde carboxymethyl cellulose (DACMC). In Chapter 3, fluorescence microclusters (MCs) were fabricated by co-assembling CSNFs and DACMC. This thesis is expected to provide different strategies for the fabrication of composites using only bio-based materials with a variety of applications to widen the design of eco-friendly materials to make a better impact for a sustainable future.

Chapter 1

pH-responsive three-dimensionally (3D) stable hydrogel composite of dialdehyde bacterial cellulose (DABC) and aqueous chitosan (CS) was fabricated in this Chapter by immobilizing CS into a dense cellulose nanofiber network of DABC through imine cross-linking followed by reduction into secondary amines. The composite showed stiffness changes in different pH conditions depending on the osmotic pressure changes created by protonation in acidic conditions and deprotonation in basic conditions. The composite suppressed the volume changes and kept 3D stability while showing stiffness changes thanks to the dense cellulose nanofiber network of DABC.

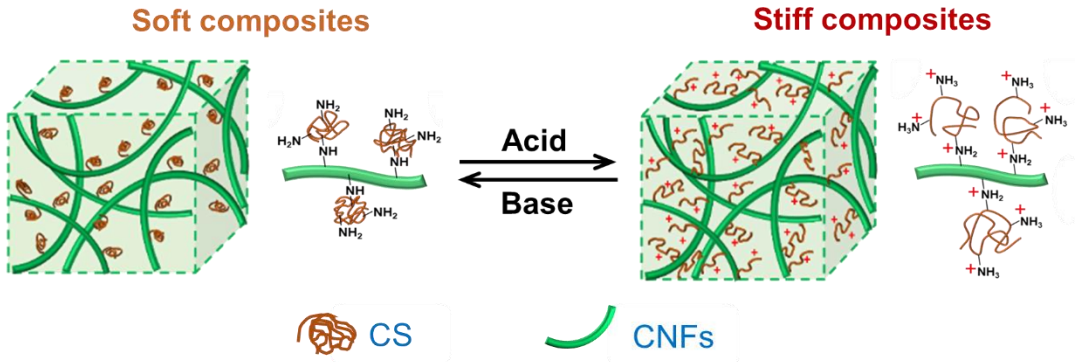

Figure 8. Schematic of the hydrogel composite of DABC-CS and the protonation difference of amino groups of CS in acidic and basic conditions.

Chapter 2

A multifunctional sponge of chitosan nanofibers (CSNFs) and dialdehyde carboxymethyl cellulose (DACMC) was fabricated by employing the freeze-thaw method. In the synthesis process, the freeze step was utilized to fabricate the 3D porous network of CSNFs and then a post-cross-linking step was performed in the thawing step to cross-link with DACMC. The material behaved as a sponge in the wet state that exhibited excellent shape recoverability continuously. The dry state sample exhibited outstanding thermal insulating and fire-retardant behavior derived from the formation of strong cross-links between CSNFs and DACMC, such as imine bonds, electrostatic

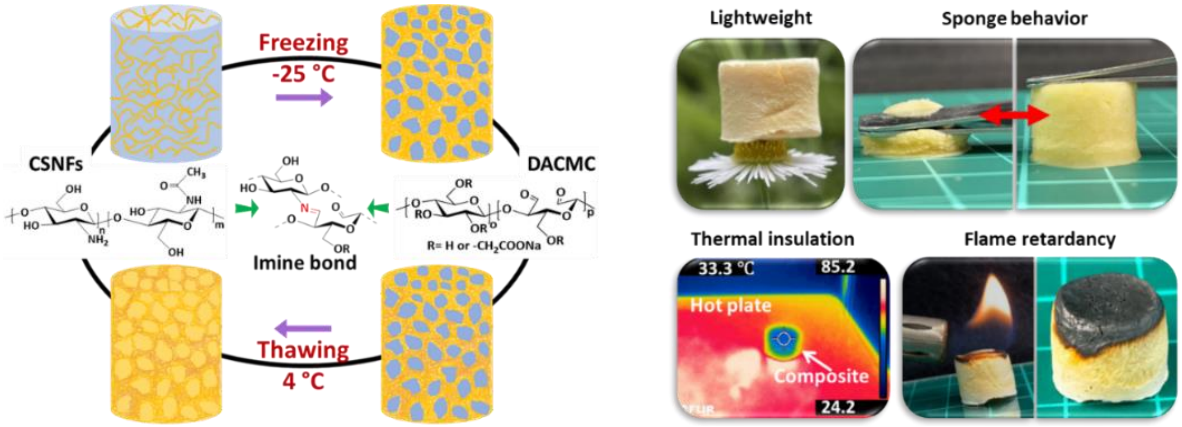

Figure 9. Schematic of the CSNFs-DACMC sponge synthesis utilizing the freeze-thaw method and the possible applications of the composite.

interactions, and hydrogen bonds**.**

Chapter 3

In this Chapter, polysaccharide-based microclusters (MCs) displaying clusterization-triggered emission (CTE) were developed. Co-assembly of chitosan nanofibers (CSNFs) and dialdehyde carboxymethyl cellulose (DACMC), cross-linked via multiple forms, enabled stable fluorescence in aqueous environments. The fabricated MCs were aggregated densely through imine bonds, electrostatic interactions, and hydrogen bonds. These various interactions between CSNFs and DACMC, result in rigid assemblies which can occur through-space interactions (TSI) followed by through-space conjugation (TSC). CTE-based fluorescence was observed in these water-stable composite

materials which were induced by TSC. A hydrogel of poly(vinyl alcohol) (PVA) was tailored into a fluorescence gel by incorporating MCs into the hydrogel matrix.

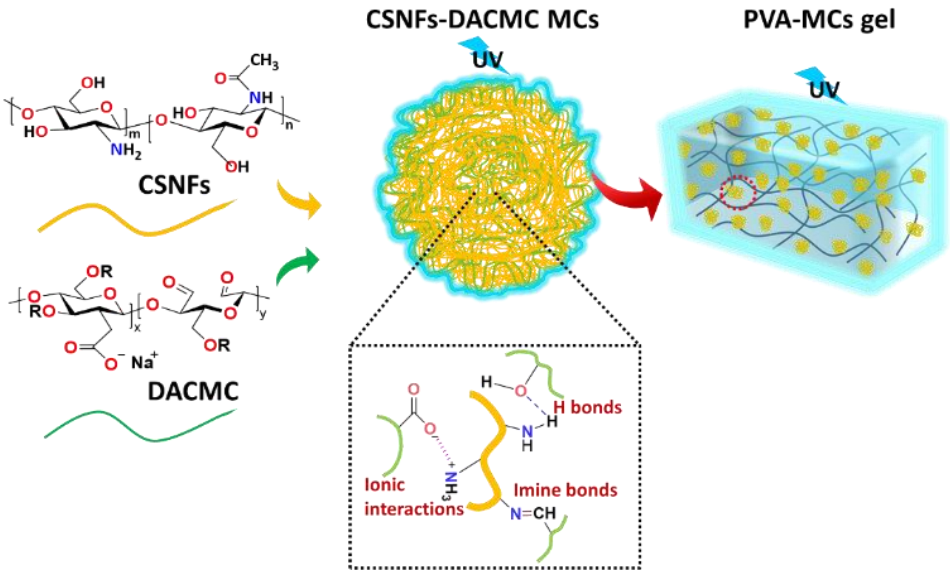

Figure 10. The schematic of the CSNFs-DACMC microcluster fabrication to induce fluorescence in hydrogel matrixes

References

(1) S.Richards, *J.Med.Oraganichem.* **2022**, *9*, 002.

(2) I. Benalaya, G. Alves, J. Lopes, L. R. Silva, *Int. J. Mol. Sci*. **2024**, *25*, 132.

(3) A. S. A. Mohammed, M Naveed, N. Jost, *J. Polym. Environ*. **2021**, *29*, 2359.

(4) E. Díaz-Montes, *Polysaccharides* **2022**, *3*, 480.

(5) C. Schuerch, *Biomedical Applications of Polysaccharides*. In Bioactive Polymeric Systems, C.G. Gebelein, C.E. Carraher, (eds). Springer, Boston, **1985**

(6) Q. Wu; N. Cheng, D. Fang, H. Wang, F.U. Rahman, H. Hao, Y. Zhang, *J. Dermatol. Sci. Cosmet. Technol.* **2024**, *1,* 100004

(7) S. Kou, L. Peters, M. Mucalo, *Carbohydr. Polym.* **2022**, *282*, 119132.

(8) D. I. Sánchez-Machado, J. López-Cervantes, M.A. Correa-Murrieta, R.G. Sánchez-Duarte, P. Cruz-Flores, G.S. la Mora-López, Chitosan. In *Nonvitamin and Nonmineral Nutritional Supplements*; M.N. Sayed, S.S. Ana (eds). Elsevier, California, **2018**.

(9) L.C. Tomé, S.C.M. Fernandes, D.S. Perez, P. Sadocco, A.J.D. Silvestre, C.P. Neto, I.M. Marrucho, C.S.R. Freire, *Cellulose* **2013**, *20*, 1807.

(10) L. Li, H. Yang, X. Li, S. Yan, A. Xu, R. You, Q. Zhang, *Carbohydr. Polym.* **2021**, *253*, 117214.

(11) S. Roy, K.L. Goh, C. Verma, B. D. Ghosh, K. Sharma, P. K. Maji, *ACS Sustain. Chem. Eng.* **2022**, *10*, 4694.

(12) E. Hajili, A. Sugawara, T.A. Asoh, H. Uyama, *ACS Sustain. Chem. Eng.* **2023**, *11*, 5473.

(13) I. Aranaz, A. R. Alcántara, M. C. Civera, C. Arias, B. Elorza, A.H. Caballero, N. Acosta, *Polymers* **2021**, *13*, 3256.

(14) M. N. V. R. Kumar, R. A. A. Muzzarelli, C. Muzzarelli, H. Sashiwa, A.J. Domb, *Chem. Rev.* **2004**, *104*, 6017.

(15) J. Wu, C. Su, L. Jiang, S. Ye, X. Liu, W. Shao, *ACS Sustain. Chem. Eng.* **2018**, *6*, 9145.

(16) T. Phaechamud, J. Charoenteeraboon, *AAPS Pharm. Sci. Tech.* **2008**, *9*, 829.

(17) M. Dellali, C. E. Iurciuc, C. L. Savin, N. Spahis, M. Djennad, M. Popa, *Molecules* **2021**, *26*, 2185.

(18) H. Haghighi, F. Licciardello, P. Fava, H. W. Siesler, A. Pulvirenti, *Food Packag. Shelf Life*. **2020**, *6,* 100551.

(19) V. G. L. Souza, J. R. A. Pires, C. Rodrigues, I. M. Coelhoso, A. L. Fernando, *Polymers* **2020**, 12, 417.

(20) L. V. Hai, L. Zhai, H. C. Kim, P. S. Panicker, D.H. Pham, J. Kim, *Nanomaterials* **2020**, **10**, 1752.

(21) J. Wang, Q. Zhou, D. Song, B. Qi, Y. Zhang, Y. Shao, Z. Shao, *J. Solgel. Sci. Technol.* **2015**, *76*, 501.

(22) M. Tan, S. Zheng, H. Lv, B. Wang, Q. Zhao, B. Zhao, *New J. Chem.* **2021**, *45*, 9829.

(23) C. Q. Ruan, M. Strømme, J. Lindh, *Carbohydr. Polym.* **2018**, *181*, 200.

(24) P. Risch, C. A. Adlhart, *ACS Appl. Polym. Mater.* **2021**, *3*, 4685.

(25) P. Risch, C. A. Adlhart, *ACS Appl. Polym. Mater.* **2021**, *3*, 4685.

(26) T. Huang, Y. Zeng, C. Li, Z. Zhou, J. Xu, L. Wang, D.-G. Yu, K. Wang, *ACS Biomater. Sci. Eng.* **2024**,

(27) Y. F. Aklog, A. K. Dutta, H. Izawa, M. Morimoto, H. Saimoto, S. Ifuku, *Int. J. Biol. Macromol.* **2015**, *72*, 1191.

(28) K. Ogura, C. Brasselet, G. Cabrera-Barjas, M. Hamidi, A. Shavandi, M. Dols-Lafargue, N. Sawamura, C. Delattre, *Materials* **2022**, *15,*1375.

(29) J. Fu, F. Yang, Z. Guo, *New J. Chem.* **2018**, *42*, 17162.

(30) A. Woźniak, M. Biernat, *J. Bioact. Compat. Polym.* **2022**, *37,* 151.

(31) T. Takigawa, Y. Endo, *JOH*. **2006**, *48*, 75.

(32) T. Jóźwiak, U. Filipkowska, P. Szymczyk, J. Rodziewicz, A. Mielcarek, *React. Funct. Polym.* **2017**, *114*, 58.

(33) S. M. Samani, F. Ahmadi, Z. Oveisi, Z. Amoozgar, *Res. Pharm. Sci.* **2015**, *10*, 1.

(34) L. Weng, X. Chen, W. Chen, *Biomacromolecules* **2007**, *8*, 1109.

(35) Y. Zhang, Y. Han, Z.A. Zhou, *Food Hydrocoll.* **2024**, *146*, 109186.

(36) L. G. Gómez-Mascaraque, J. A. Méndez, M. Fernández-Gutiérrez, B. Vázquez, J. San Román, *Acta Biomater.* **2014**, *10*, 798.

(37) F. Chen, M. Tian, D. Zhang, J. Wang, Q. Wang, X. Yu, X. Zhang, C. Wan, *Mater. Sci. Eng. C* **2012**, *32*, 310.

(38) A. D. Rogalsky, H. J. Kwon, P. Lee-Sullivan, *J. Biomed. Mater. Res. A* **2011**, *99*, 367.

(39) X. Li, Y. Weng, X. Kong, B. Zhang, M. Li, K. Diao, Z. Zhang, X. Wang, H. Chen, *J. Mater. Sci. Mater. Med.* **2012**, *23*, 2857.

(40) J. Zhu, G. Jiang, W. Hong, Y. Zhang, B. Xu, G. Song, T. Liu, C. Hong, L. Ruan, *Mater. Sci. Eng. C* **2020**, *117*, 111273.

(41) N. T. P. Nguyen, L. V. H. Nguyen, N. M. P. Tran, D. T. Nguyen, T. N. T. Nguyen, H. A. Tran, N. N. T. Dang, T. V. Vo, T. H. Nguyen, *Mater. Sci. Eng C* **2019**, *103*,109670.

(42) S. Liu, N. Jiang, Y. Chi, Q. Peng, G. Dai, L. Qian, K. Xu, W. Zhong, W. Yue, *ACS Biomater. Sci. Eng.* **2022**, *8*, 3754.

(43) J. Ranjbar, M. Koosha, H. Chi, A. Ghasemi, F. Zare, M. A. Abdollahifar, M. Darvishi, Li, *Cellulose* **2021**, *28*, 3663.

(44) C. Sheng, Y. Zhou, J. Lu, X. Zhang, G. Xue, *Polym. Compos.* **2019**, *40*, 2432.

(45) F. Mushtaq, M. Ashfaq, F. Anwar, B. T. Ayesha, H. S. Latif, S. Khalil, H. S. Sarwar, M. I. Khan, M. F. Sohail, I. Maqsood, *ACS Omega* **2024**, *9*, 2145.

(46) M. F. Ahmad, S. Hassan, Z. Imran, D. Mazhar, S. Afzal, S. A. Ullah, *J. Polym. Environ.* **2024**, *32*, 194.

(47) K. Zhang, S. Yan, G. Li, L. Cui, J. Yin, *Biomaterials* **2015**, *71*, 24.

(48) K. Zafeiris, D. Brasinika, A. Karatza, E. Koumoulos, I. K. Karoussis, K. Kyriakidou, C. Charitidis, *Mater. Sci. Eng. C* **2021**, *119*, 111639.

(49) R. Panchal, T. Mateti, K. Likhith, F. C. Rodrigues, G. Thakur, *React. Funct. Polym.* **2022**, *178*, 105339.

(50) M. E. Frohbergh, A. Katsman, G. P. Botta, P. Lazarovici, C. L. Schauer, U. G. K. Wegst, P. I. Lelkes, *Biomaterials* **2012**, *33*, 9167.

(51) A. Subramanian, H. Y. Lin, H. *J. Biomed. Mater. Res. A* **2005**, *75*, 742.

(52) T. Jóźwiak, U. Filipkowska, P. Szymczyk, J. Rodziewicz, A. Mielcarek, *React. Funct. Polym.* **2017**, *114*, 58.

(53) A. Jawad, M. Aazmi, B. Shafiq, A. Jawad, *Science Letters* **2020**, *14*, 1.

(54) P. R. Chang, R. Jian, J. Yu, X. Ma, *Food Chem.* **2010**, *120*, 736.

(55) K. Yan, Y. Wan, F. Xu, J. Lu, C. Yang, X. Li, Z. Lu, X. Wang, D. Wang, D. *Carbohydr. Polym.* **2023**, *302*, 120427.

(56) K. Baysal, A. Z. Aroguz, Z. Adiguzel, B. M. Baysal, *Int. J. Biol. Macromol.* **2013**, *59*, 342.

(57) H. Seddiqi, E. Oliaei, H. Honarkar, J. Jin, L.C. Geonzon, R.G. Bacabac, J. Klein-Nulend, *Cellulose* **2021**, *28*, 1893.

(58) B. Guo, W. Chen, L. Yan, *ACS Sustain. Chem. Eng.* **2013**, *1*, 1474.

(59) T. Aziz, A. Farid, F. Haq, M. Kiran, A. Ullah, K. Zhang, C. Li, S. Ghazanfar, H. Sun, R. Ullah, A. Ali, M. Muzammal, M. Shah, N. Akhtar, S. Selim, N. Hagagy, M. Samy, S. K. Al Jaouni, *Polymers* **2022**, *14*, 3206.

(60) R. de Avila Delucis, P. H. G. de Cademartori, A. R. Fajardo, S. C. Amico, *Cellulose and Its Derivatives, In Polysaccharides: Properties and Applications, 1,* Inamuddin, M I. Ahamed, R. Boddula, T. Altalhi, (eds), Scrinvener, **2021**.

(61) S. Gea, Marpongahtun, D. Y. Nasution, K. M. Pasaribu, R. M. Tambunan, A. F. Piliang, M. S. Karina, *Afr. J. Chem. Eng.* **2023**, *46*, 277.

(62) A. Balea, E. Fuente, M. C. Monte, N. Merayo, C. Campano, C. Negro, A. Blanco, *Molecules* **2020**, *25*, 526.

(63) C. Felgueiras, N. G. Azoia, C. Gonçalves, M. Gama, F. Dourado, *Front. Bioeng. Biotechnol.* **2021**, *9*, 608826.

(64) A. Cristiane, K. Bierhalz, *Cellulose Chem. Technol.* **2021***, 55,* 725.

(65) H. Du, W. Liu, M. Zhang, C. Si, X. Zhang, B. Li, *Carbohydr. Polym.* **2019**, *209,* 130.

(66) B. Joseph, V. K. Sagarika, C. Sabu, N. Kalarikkal, S. Thomas, *J. Bioresour. Bioprod.* **2020**, *5*, 223.

(67) A. J. Brown, *J. Chem. Soc., Trans.***1886,** *49, 432.*

(68) W. Liu, H. Du, M. Zhang, K. Liu, H. Liu, H. Xie, X. Zhang, C. Si, *ACS Sustainable Chem. Eng*. **2020**, *8*, 7536.

(69) C. Qian, T.A. Asoh, H. Uyama, *J. Mater. Chem. B* **2020**, *8*, 2400.

(70) P. Kotcharat, P. Chuysinuan, T. Thanyacharoen, S. Techasakul, S. Ummartyotin, *Sustain Chem. Pharm.* **2021**, *20*, 100404.

(71) Y. Hou, X. Wang, J. Yang, R. Zhu, Z. Zhang, Y. Li, *J. Biomed. Mater. Res. A* **2018**, *106*, 1288.

(72) S. Gorgieva, S. Hribernik, *Nanomaterials* **2019**, *9*, 303.

(73) P. Weyell, U. Beekmann, C. Küpper, M. Dederichs, J. Thamm, D. Fischer, D. Kralisch, D. *Carbohydr. Polym.* **2019**, *207*, 1.

(74) Q. Xu, Y. Ji, Q. Sun, Y. Fu, Y. Xu, L. Jin, *Nanomaterials* **2019**, *9* 253.

(75) J. E. Arikibe, R. Lata, K. Kuboyama, T. Ougizawa, D. Rohindra, *ChemistrySelect* **2019**, *4*, 9915.

(76) R. Drozd, M. Szymańska, R. Rakoczy, A. Junka, P. Szymczyk, K. Fijałkowski, *Appl. Biochem. Biotechnol.* **2019**, *187*, 176.

(77) Y. Hu, F. Liu, Y. Sun, X. Xu, X. Chen, B. Pan, D. Sun, J. Qian, *J. Chem. Eng.* **2019**, *371*, 730.

(78) M. S. Rahman, M. S. Hasan, A. S. Nitai, S. Nam, A. K. Karmakar, M. S.Ahsan, M. J. A. Shiddiky, M. B. Ahmed, *Polymers* **2021**, *13*, 1345.

(79) A. Zennifer, P. Senthilvelan, S. Sethuraman, D. Sundaramurthi, *Carbohydr. Polym.* **2021**, *256*, 117561.

(80) Y. Ogushi, S. Sakai, K. Kawakami, *J. Biosci. Bioeng.* **2007**, *104*, 30.

(81) A. Pettignano, A. Charlot, E. Fleury, *Polymer Reviews* **2019**, *59*,510.

(82) M. N. Nadagouda, R. S. Varma, *Biomacromolecules* **2007**, *8*, 2762.

(83) M. Yildirim-Yalcin, F. Tornuk, O. S. Toker, *Trends Food Sci. Technol.* **2022**, *129*, 179.

(84) H. Krizova, J. Wiener, *AUTEX RES J.* **2013**, *13*, 33.

(85) G. Dalei, S. Das, M. Pradhan, *Cellulose* **2022**, *59*, 5429.

(86) I. A. Duceac, F. Tanasa, S. Coseri, *Materials* **2022**, *15*, 5076.

(87) J. Simon, L Fliri, F. Drexler, M. Bacher, J. Sapkota; M. Ristolainen, M. Hummel, A. Potthast, T. Rosenau, *Carbohydr. Polym.* **2023**, *310*, 120691.

(88) U. J. Kim, S. Kuga, M. Wada, T. Okano, T. Kondo, *Biomacromolecules* **2000**, *1*, 488.

(89) M. Wu, S Kuga, *J Appl. Polym. Sci.* **2006**, *100*, 1668.

(90) U. J. Kim, S. Kuga, *J. Chromatogr. A* **2001**, *919*, 29.

(91) W. Kasai, M. Ek, T. Morooka, *Cellulose* **2014,** *21, 769.*

(92) A. Lucia, M. Bacher, H. W. G. Van Herwijnen, T. Rosenau, *Molecules* **2020**, *25*, 2458.

(93) D. Rajalaxmi, N. Jiang, G. Leslie, A. J. Ragauskas, *Carbohydr. Res.* **2010**, *345*, 284.

(94) E. S. A. El-Sayed, S. Dacrory, H.A. Essawy, H. S. Ibrahim, N. S. Ammar, S. Kamel, *BMC Chem.* **2023**, *17*, 117.

(95) F. Dong, S Li, *Polymers (Basel)* **2018**, *10*, 673.

(96) K. Wegrzynowska-Drzymalska, D. T. Mlynarczyk, D. Chelminiak-Dudkiewicz, H. Kaczmarek, T. Goslinski, M. Ziegler-Borowska, *Int. J. Mol. Sci.* **2022**, *23,* 9700.

(97) D. George, P. U. Maheswari, K. M. M. Sheriffa Begum, G. J. Arthanareeswaran, *Agric. Food Chem.* **2019**, *67*, 10880.

(98) S. Káčerová, M. Muchová, H. Doudová, L. Münster, B. Hanulíková, K. Valášková, V. Kašpárková, I. Kuřitka, P. Humpolíček, Z. Víchová, O. Vašíček, J. Vícha, *Carbohydr Polym.* **2024**, *327*, 121640.

Chapter 1

Stimuli-Responsive Composite Hydrogels with Three-Dimensional Stability Prepared Using Oxidized Cellulose Nanofibers and Chitosan

1-1. Introduction

Stimuli-responsive hydrogels are smart materials that change their mechanical and/or physical properties in response to external stimuli such as temperature, pH, electric fields, magnetic fields, and light.[1,2] They also display similarities to living organisms regardless of whether the hydrogels are derived naturally or from synthetic polymers.[3] There are many biomedical applications making use of these intelligent hydrogels, such as artificial tissues, medical implants,[4,5] 3D cell encapsulation, drug delivery, and cell proliferation, as well as other fields including shape memory mechanisms, supramolecular switches, soft actuators, and sensors.[6] The mechanical property responses of hydrogel composites have been developed primarily by tuning cross-linking in hydrogel networks using different stimuli and managing swelling and shrinking behavior.[7]

In biomedical applications, such as gastrointestinal tract and tumoral culture applications, pH-responsive hydrogels have been attracting increasing attention.[8,9] Such pH responsiveness has been developed using polymer materials with acidic or basic groups that can accept or release protons under certain pH conditions.[10,11] Accordingly, pH-responsive hydrogels change their physical properties by changing the affinity of the polymer to solvents, charge density, osmotic pressure, and cross-linking density of the polymer.[12] Biomedical applications, such as sustainable drug delivery, disease diagnosis, and biosensors, are the fields most commonly utilizing these hydrogel composites.[13] Other applications include wastewater treatments, dye adsorption, and implantable devices,[14] almost all of which rely heavily on the swelling-deswelling properties of the hydrogel. Although the swelling behavior of hydrogels is advantageous in some applications, such as soft actuators and temporary scaffolds, it can cause undesirable nerve compression, neighboring tissue damage, and displacement from the installation sites due to concurrent, extreme swelling and shrinking.[15] Consequently, it is important to develop a design that allows for variable hydrogel stiffness while maintaining its three-dimensional stability.

Recently, the synthesis of stimuli-responsive hydrogel complexes using bacterial cellulose (BC) has attracted much attention.[16] A composite hydrogel with the ability to change its stiffness based on ionic strength was developed using BC grafted with poly(sodium styrene sulfonate) (PSS). BC acts as a dense matrix, the PSS causing its responsiveness to different ionic strengths. The composite has exhibited good three-dimensional stability which is credited to the network structure of BC preventing the potential swelling and shrinkage.[6] A dual pH-responsive and mechanically adaptive hydrogel composite has been synthesized with squat actuating capability. Poly(acrylic acid) (PAA) and poly(2-(dimethylamino)ethyl methacrylate) were grafted with BC in this synthesis. Synthetic polymers have also been used in these BC fabrications.[17]

This study focused on preparing pH-responsive hydrogel composites with three-dimensional stability using only natural polymers. Employing the surface modification of chitosan onto the oxidized cellulose nanofiber (CNF) surface of dialdehyde bacterial cellulose (DABC), DABC/chitosan composite gel was successfully prepared, demonstrating stiffness changes in response to pH without any volumetric change of the gels.

1-2. Experimental Section

Materials and Methods

Bacterial cellulose (BC) pellicles were purchased from Fujiko. Co., Ltd. Chitosan 100 kDa, acetic acid, sodium hydroxide (NaOH), hydrochloric acid (HCl), and sodium chloride (NaCl) were purchased from Wako Chemicals. Sodium periodate ($NaIO_4$), phosphate buffer saline solution (pH 7.4), and hydroxylamine hydrochloride (HAHCl) were purchased from Nacalai Tesque Inc. All solutions were made using deionized (DI) water.

Purification of BC

First, the bacterial cellulose (BC) pellicles were added with DI water and stirred for two days to wash. Water was changed hourly more than 15 times. Then, 0.2 mol/L NaOH aqueous solutions were used to further remove bacterial cell walls from the BC at 80 °C for 4 hours. Next, the samples were washed with DI water until the washings became neutral to universal pH paper. The cellulose content of the BC was quantified to be 1 wt% and the water content was 99 wt% by drying at 80 °C

in an oven. The drying was done until a constant weight was given to the time-to-time weight measurements.[17]

Oxidation of Bacterial cellulose

Bacterial cellulose (BC) oxidation was conducted according to some literature with modifications.[18] The oxidation of the BC was optimized under different conditions such as temperature, the molar ratio between the oxidant and the cellulose, the concentration of the oxidant, and the oxidation time. Then samples were oxidized with the optimized conditions. First, 3.5 g of $NaIO_4$ was dissolved in 120 mL of DI water to obtain a 3 wt% solution, after which 100.0 g of BC was immersed in the solution, the container then being covered with aluminum foil. The molar ratio of the oxidant to BC was 3:1. The reaction mixture was kept at 25 °C for 24 hours. Subsequently, the reaction was quenched by adding 5 mL of ethylene glycol and was kept for another 30 minutes. The oxidized sample was then washed with DI water for a day, changing the water hourly.

Determination of the aldehyde content

The degree of oxidation (DO) was considered as the molar ratio of oxidized hydroxyl groups to the cellulose units. 1.0 g of the DABC is taken and cut into small pieces. Next, 10 mL of DI water was added and stirred well, after which 1 mol/L HCl was used to adjust the pH value to 3. Subsequently, 0.5 g of hydroxylamine hydrochloride was added to the sample and dissolved. The sample was kept overnight and back titration was done using 0.05 mol/L NaOH aqueous solvent. The aldehyde content was calculated using equation (1), where *DO* is the degree of oxidation, *V* is the volume of NaOH, *C* is the concentration of NaOH solution, and *m* is the user weight of the DABC:

$$DO = \frac{CV}{m/162} \quad (1)$$

Composition of dialdehyde bacterial cellulose (DABC) with chitosan

Composites of dialdehyde bacterial cellulose (DABC) and chitosan were produced using a pH-exchanging method. First, the DABC was mixed with chitosan in an acidic pH medium and then a neutral pH media was supplied with a phosphate-buffered saline (PBS) solution. One gram of Chitosan was dissolved in 100 mL of 1 wt% acetic acid aqueous solution. The solution was stirred

for one night for complete hydration of the polymer. Next, the solution was filtered to remove the insoluble polymer particles. The pH value of the solution was checked and was found to have a pH of approximately 4. Purified DABC cubes were then immersed in the chitosan solution and the mixture was shaken for two days at 25 °C. After two days the composites were removed and then kept in a buffer solution of pH 7.4 for another two days, after which the composites were washed with DI water. To reduce the formed imine bonds into secondary amine groups, the composites were reacted with 0.01 mol/L $NaBH_3CN$ solutions at 10 °C for 24 h. Finally, the composites were washed with DI water for one day, refreshing the water hourly.

Composited polymer content determination

Pure dialdehyde bacterial cellulose (DABC-0) and composited dialdehyde bacterial cellulose (DABC-CS-amine) were dried in an oven at 80 °C temperature. The drying was done until a constant weight was given to the time-to-time weight measurements (the wet weight of the materials being obtained before drying).[19] The water and polymer contents of the composites were calculated using equations (2) and (3) where R_w is the water content, R_C is the cellulose content, R_P is the polymer content, W_d is the dry weight of the composites, W_0 is the wet weight of the composites, and W_c is the cellulose amount in the DABC. The W_c of the composites was calculated using the W_c of the pure DABC as it is difficult to determine it in the composites themselves.

$$R_w = \frac{(W_0 - W_d)}{W_0} 100 \quad (2)$$

$$R_{wc} = \frac{W_c}{W_0} 100 \quad (3)$$

$$R_p = \frac{W_d - W_c}{W_0} 100 \quad (4)$$

The mechanical strength and the three-dimensional stability of the composites

The mechanical strength was checked by compressing the composites along the growing direction where the mechanical strength was lower. A 100 N load was supplied at a rate of 3.0 mm/min using a universal testing machine (UTM) (Shimadzu EZ Graph, Japan). The three-dimensional stability of the composites was tested by considering the volumetric change in the composites. The volumes of the samples at all characterization steps were obtained using the water displacement in a measuring cylinder. Any excess solvent on the outer surfaces of the samples was

gently removed using dry tissue paper. Equation 5 was used to calculate the volume change ratio (*VCR*), where V_i is the initial volume of the samples and V_f is the final volume.

$$VCR = \frac{(V_f - V_i)}{V_i} 100 \quad (5)$$

The behavior of the composites at different pH environments

Aqueous solutions at different pH values that is, 2, 3, 4, 5, 6, 7, 8, 9, and 10 with similar ionic strengths were prepared using 0.01 mol/L HCl, 0.01 mol/L NaOH, and 0.01 mol/L NaCl solutions. Composited samples were immersed in these solutions for 48 hours at 25 ℃. Next, the samples were subjected to a compression test, with Young's modulus being calculated for each sample and the strain at 0.05 MPa being calculated. Moreover, the polymer content of each sample and the *VCR* were determined.

Characterization of the hydrogel composite

The progress of chemical crosslinking was determined using attenuated total reflection Fourier transform infrared (ATR-FTIR) spectroscopy (Thermo Scientific Nicolet iS 5, USA). The composites were frozen by immersion in liquid nitrogen and then dried under vacuum. The FTIR spectrums of bacterial cellulose, chitosan (CS), dialdehyde bacterial cellulose (DABC), DABC-CS-imine, and DABC-CS-amine were obtained from the inside and outside of the samples. The morphology of the composites was observed using scanning electron microscopy (SEM) (Hitachi SU3500, Japan). A comparison of the appearance of the cellulose nanofiber arrangement was conducted on all the materials and composites. Freeze-dried samples were observed under an accelerating voltage of 15.0 kV and a high vacuum environment after which they were sputtered for gold-palladium using an MSP-1S magnetron sputter (Vacuum Device Inc., Japan).

1-3. Results and Discussion

The dialdehyde bacterial cellulose (DABC)/chitosan (CS) composite gels were prepared by surface modification of chitosan onto the cellulose nanofibers of DABC. Since the oxidation reduces the crystallinity of the cellulose polymer, size reduction due to the dissolving of the

oxidized polymer chains occurs. Subsequently, oxidation optimization was performed to minimize the size reduction of the material with a high degree of oxidation. As the cubic structure of the bacterial cellulose (BC) is a dense network of cellulose nanofibers (CNFs), the oxidation should be done at a slower rate to confirm the even oxidation of the cube. Even oxidation of the BC was colorimetrically proved by the reaction of 2,4-Dinitrophenylhydrazene with dialdehyde bacterial cellulose (DABC), seen as an even coloration. Moreover, the reaction of DABC with hydroxylamine hydrochloric acid was used to determine the degree of oxidation (DO) by pH titration. The maximum DO was ≈24% for the optimized oxidation conditions.

The reaction between the aldehyde groups of dialdehyde bacterial cellulose (DABC) and primary amine groups of chitosan (CS) causes imine bonds to prepare BC/CS composites (DABC/CS-imine) (**Figure 1-1a**). In this reaction, chitosan solutions are prepared using acetic acid. Imine bonds are stable in neutral and basic conditions but unstable in acidic conditions. However, the successful composition of chitosan with DABC under better reaction conditions can still be difficult. For example, the maximum pH value that could be obtained in the chitosan

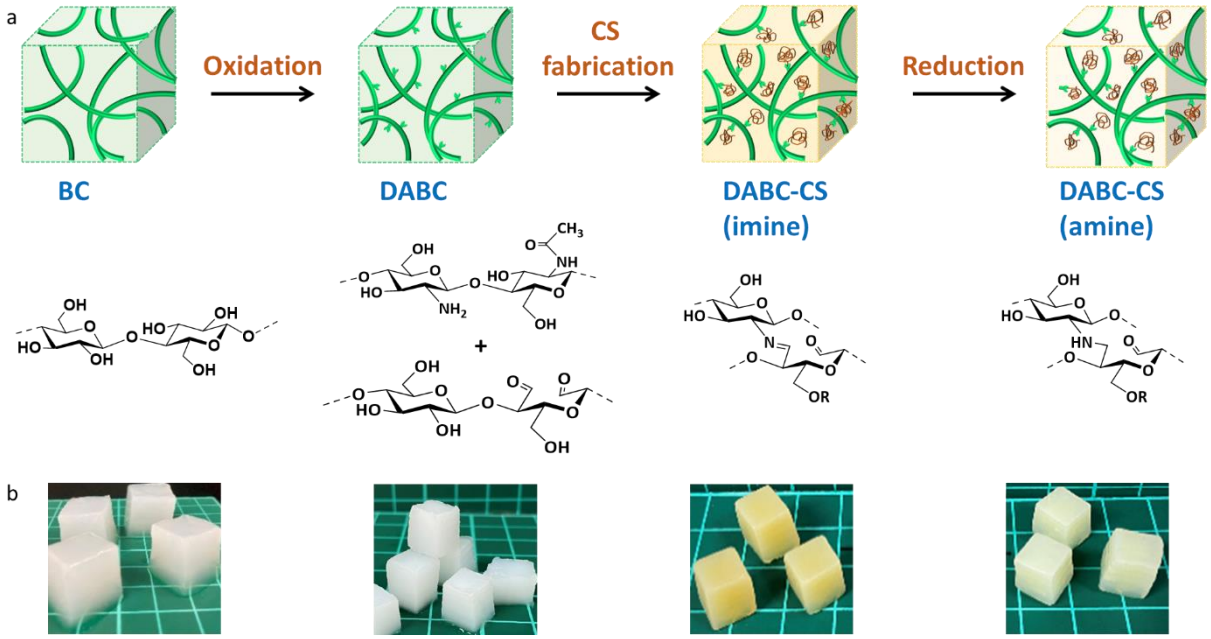

Figure 1-1. (a) Schematic illustration of the fabrication process of DABS-CS hydrogel composite and the chemical structures of the materials in each step. (b) Photographs of the resulting materials in each step.

solution was 6.1, but even when the composition was performed at a pH of 6.1, it was not successful inside the DABC cube, the dense network structure of the DABC cube preventing the

polymer chains from penetrating inside the cube after the outer surface was composited with the polymer. Consequently, a pH exchange composition was used in this work. First, the chitosan solution was mixed with the dialdehyde bacterial cellulose (DABC) cubes in acidic pH conditions (a pH of 4) where the possibility of imine bond formation was low and unstable. Next, the sample was kept in a PBS buffer solution of pH 7.4, a better pH condition for imine bond formation. In this way, chemical crosslinking made it possible to composite chitosan evenly in the DABC network matrix. Imine bonds were then reduced into secondary amines (DABC-CS-amine) (**Figure 1-1a**) as imine bonds are not stable in acidic conditions. **Figure 1-1b** shows the appearance of the bacterial cellulose cubes after each reaction step. Although the volume decreased slightly due to oxidation, the shape of the cube was maintained in all cases.

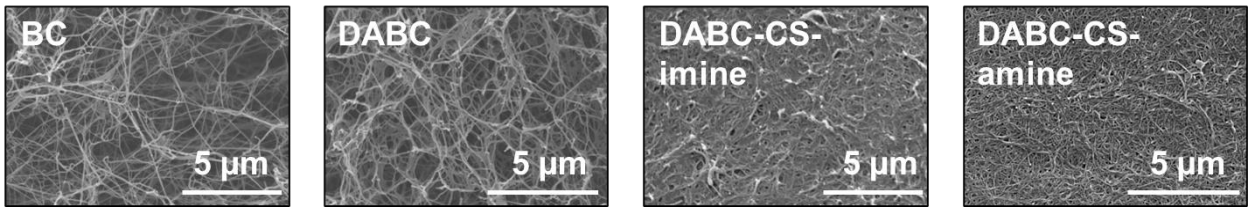

Figure 1-2. SEM images of BC, DABC, DABC-CS-imine, and DABC-CS-amine from left to right.

The internal structure of the bacterial cellulose (BC) and BC composite was observed using SEM. The BC interior structure was made up of ultra-fine cellulose nanofibers oriented into different angles to create a dense 3D network with a porous structure. After oxidation, dialdehyde bacterial cellulose (DABC) still maintains a porous network structure. However, we confirmed dense network structures by reaction with chitosan, although similar structures were obtained before and after reduction. This may be due to the agglomeration of the cellulose nanofibers (CNFs) during the drying process due to the chemically modified chitosan on the surface of the CNFs acting as a binder (**Figure 1-2**). In any case, the fiber structure of the CNFs was maintained, indicating that the BC and chitosan had successfully combined.

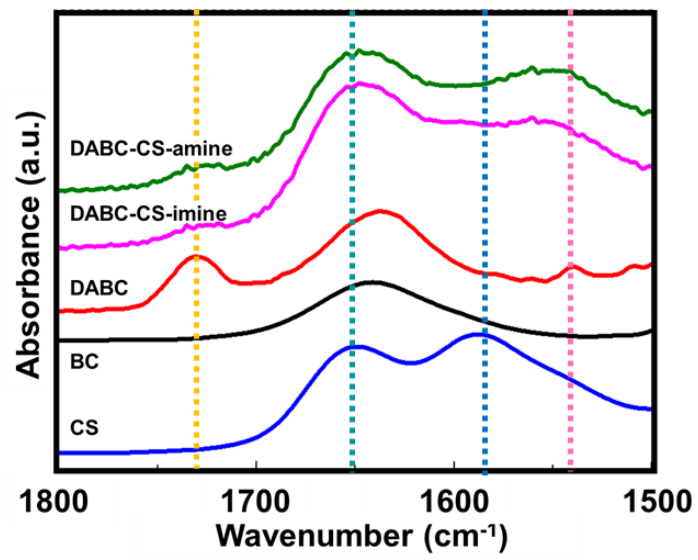

Figure 1-3. FRIR spectra of CS, BC, DABC, DABC-CS-imine, and DABC-CS-amine.

Each chemical reaction was studied using FTIR spectra (**Figure 1-3**). A clear peak separation was observed at 1735 cm^{-1} for the stretching vibrations of the carbonyl groups of aldehydes, which is not shown in the FTIR spectrum of bacterial cellulose (BC), indicating successful oxidation. The intensity of the carbonyl peak was largely reduced in dialdehyde bacterial cellulose-chitosan (DABC-CS-imine), indicating imine formation. The FTIR of chitosan showed a broad peak around 1590 cm^{-1} for the bending vibration of the N-H bond of primary amine. This peak intensity has been reduced and significantly shifted (to 1554 cm^{-1}) in the composite FTIR spectrum. Although imine and secondary amine bond formation are both difficult to identify using FTIR spectra, these results support the chemical bond formation by consuming aldehyde groups. Chitosan was retained in the bacterial cellulose by reduction to secondary amines, while it would have diffused out of the composite if the imine bond had not been reduced, suggesting that the reaction was proceeding.

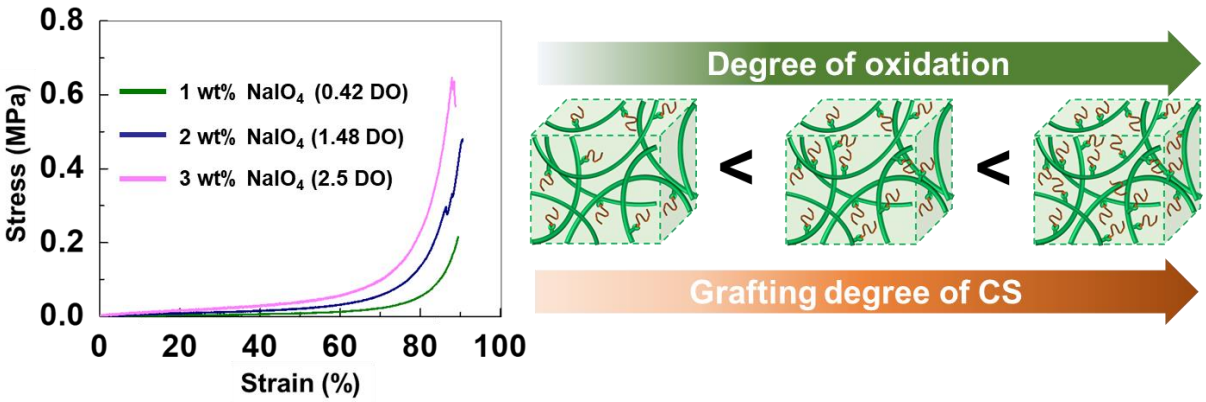

Figure 1-4. Stress-strain curves of DABC-CS-amine composites in different DO values (mmol/g) and the graphical illustration of the relationship of mechanical strength and DO

DABC-CS-amine was prepared using dialdehyde bacterial cellulose of different oxidation degrees and its mechanical strength was evaluated by compression. As shown in **Figure 1-4**, the mechanical strength increased when the amount of aldehyde groups increased due to increasing grafting chitosan. This is because chitosan, which is partially dissolved by the chemical modification of cellulose, increases osmotic pressure and improves mechanical strength.

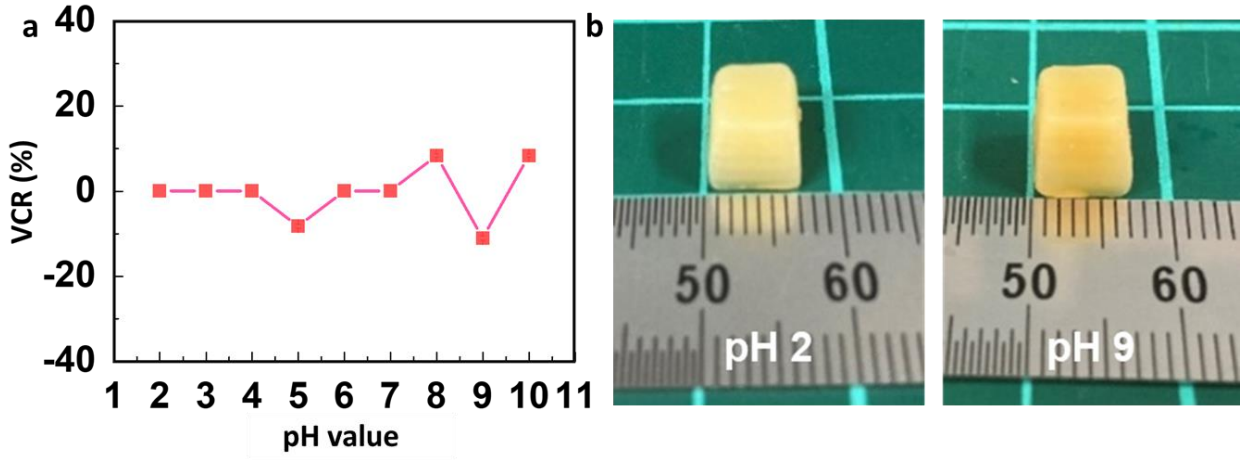

Figure 1-5. VCR of DABC-CS-amine composites in different pH conditions and photographs of the composites immersed in pH 2 and pH 10 aqueous solutions.

Primary amine groups in the chitosan polymer chains and also the secondary amine groups in the modified site can be protonated in acidic conditions. In normal hydrogels, ionization causes swelling due to the driving force of osmotic pressure from ionic units. However, composites could maintain their three-dimensional stability under all the pH conditions from acidic to basic, the maximum volume change ratio (VCR) being approximately 10% (**Figure 1-5a**) the present BC-CS-amine composite appeared almost the same at pH 2 and pH 9 across the p*K*a (6.5) of chitosan (**Figure 1-5b**). This is because the highly intertwined nanofiber network of bacterial cellulose inhibits the protonation-induced swelling and deprotonation-induced shrinkage of chitosan.

When compared with the previous works which have used chitosan crosslinked with glutaraldehyde,[20] or oxidized polysaccharides they all show swelling properties responding to pH changes on a large scale.[21,22]

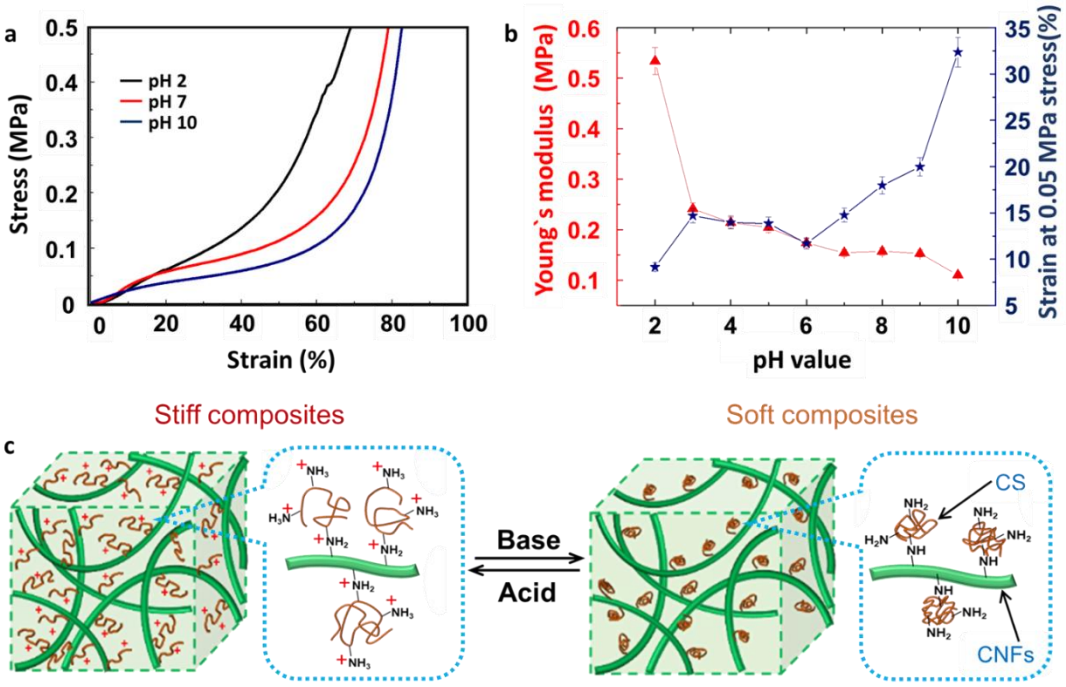

Figure 1-6. (a) Stress-strain compression spectra of DABC-CS-amine composites immersed in different pH aqueous solutions. (b) The graph of Young`s modulus and the strain at 0.05 MPa stress in different pH conditions. (c) The graphical illustration of the osmotic pressure changes of the composite due to the protonation difference.

Although the apparent volume remained almost the same, the mechanical strength changed markedly in response to pH as shown in **Figure 1-6**. Young's modulus and strain at a stress of 0.05 MPa are shown as indices of stiffness. If the strain is high when the same stress is applied, it means that the material is soft. It can be seen that Young's modulus decreases, and the strain increases as the pH is increased from pH 2 to pH 9 (**Figure 1-6b**). The proportion of the protonation changes with the pH value. The protonated stiff gel in the highly acidic conditions gradually softens by deprotonation with the pH value increased. In pH 2 composites showed the highest mechanical strength due to high protonation. Also, composites became very brittle, and composite structure was broken showing plastic deformation during the compression. With the pH value increasing composites showed elastic properties during the compression. Moreover, within these conditions, the quantity of chitosan polymer was stable (around 13 mg/g cellulose) in a considerable range inside the composites.

1-4. Conclusions

Stimuli-responsive all-polysaccharide composites were effectively prepared by combining cellulose nanofibers and chitosan. The matrix utilized dialdehyde bacterial cellulose, a highly intertwined cellulose nanofiber network, to immobilize chitosan by forming imine bonds, which were reduced to secondary amines. The mechanical property changes of the composites were examined in relation to pH variations, revealing stiff mechanical properties under acidic conditions and soft properties under basic and neutral conditions due to osmotic pressure changes. During the pH-responsive process, the volume change of the composites was suppressed, maintaining three-dimensional stability due to the rigid cross-linked network of dialdehyde bacterial cellulose acting as a supportive material. These environmentally and biologically friendly, stimuli-responsive, and dimensionally stable composite materials, composed solely of polysaccharides, are expected to find increasing applications as biomaterials.

1-5. References

(1) M.C. Catoira, L. Fusaro, D. Di Francesco, M. Ramella, F. Boccafoschi, *J. Mater. Sci. Mater. Med.* **2019**, *30*, 115.

(2) L. Montero De Espinosa, W. Meesorn, D. Moatsou, C. Weder, *Chem. Rev.* **2017**, *117*, 12851.

(3) M. C. I. Mohd Amin, N. Ahmad, M. Pandey, C. Jue Xin, *Drug Dev. Ind. Pharm.* **2014**, *40*, 1340.

(4) Q. Shi, H. Liu, D. Tang, Y. Li, X. J. Li, F. Xu, *NPG Asia Mater.* **2019**, *64*, 11.

(5) Z. Wang, J. Wang, J. Ayarza, T. Steeves, Z. Hu, S Manna, Esser-Kahn, A. P. *Nat. Mater.* **2021**, *20*, 869.

(6) C. Qian, T. A. Asoh, H. Uyama, *Chem. Commun.* **2018**, *54*, 11320.

(7) M. A. C. Stuart, W. T. S. Huck, J. Genzer, M. Müller, C. Ober, M. Stamm, G. B. Sukhorukov, I. Szleifer, V. V. Tsukruk, M. Urban, F. Winnik, S. Zauscher, I. Luzinov, S. Minko, *Nature Mater.* **2010**, *9*, 101.

(8) C. Jin, W. Song, T. Liu, J. Xin, W. C. Hiscox, J. Zhang, G. Liu, Z. Kong, *ACS Sustain. Chem. Eng.* **2018**, *6*, 1763.

(9) X. Shi, Y. Zheng, C. Wang, L. Yue, K. Qiao, G. Wang, L. Wang, H. Quan, *RSC Adv.* **2015**, *5*, 41820.

(10) J. C. Kurnia, E. Birgersson, A.S. Mujumdar, *Polymer* **2012**, *53*, 613.

(11) X. J. Liu, H. Q. Li, B. Y. Zhang, Y. J. Wang, X. Y. Ren, S. Guan, G. H. H. Gao, *RSC Adv.* **2016**, *6*, 4850.

(12) U. Yildiz, Ö. F. B. Kemik, B. Hazer, *J. Hazard. Mater.* **2010**, *183*, 521.

(13) X. Qi, W. Wei, J. Li, G. Zuo, X. Pan, T. Su, J. Zhang, W. Dong, *Mol. Pharm.* **2017**, *14*, 43.

(14) R. Singh, D. Pal, S. Chattopadhyay, *ACS Omega* **2020**, *5*, 21768.

(15) H. Kamata, K. Kushiro, M. Takai, U. Chung, T. Sakai, *Angewandte Chemie.* **2016**, *128*, 9428.

(16) A. Sharma, M. Thakur, M. Bhattacharya, T. Mandal, S. Goswami, *Biotechnol. Rep*. **2019**, *21*, 316.

(17) C. Qian, T. A. Asoh, H. Uyama, *Macromol. Rapid Commun.* **2020***, 41, 2000406.*

(18) U. J. Kim, S. Kuga, M. Wada, T. Okano, T. Kondo, *Biomacromolecules* **2000**, *1*, 488.

(19) C. Qian, T. A. Asoh, H. Uyama, *J. Mater. Chem. B* **2020**, *8*, 2400.

(20) G. Martínez-Mejía, N. A. Vázquez-Torres, A. Castell-Rodríguez, J. M. del Río, M. Corea, R. Jiménez-Juárez, *Colloids. Surf. A Physicochem. Eng. Asp.* **2019**, *579*.

(21) F. Li, W. G. Liu, K. De Yao, *Biomaterials* **2020***, 23,* 343.

(22) D. Wei, Q. Liu, Z. Liu, J. Liu, X. Zheng, Y. Pei, K. Tang, *Int. J. Biol. Macromol.* **2019**, *135*, 561.

Chapter 2

Multifunctional Chitosan Nanofiber-Based Sponge Materials Using Freeze-Thaw and Post-Cross-Linking Method

2-1. Introduction

Sponges are defined as fibrous porous materials featuring three-dimensional (3D) networks that display reversible compressibility, mechanical integrity, and low specific gravity. These materials are characterized by their breathability, low density, and substantial pore volume, enabling the integration of various functional properties, thus enhancing their versatility for multiple applications.[1] The synthesis of sponge materials commonly employs techniques such as electrospinning, particulate leaching, freeze-casting, and thermally induced phase separation.[2] The prevalent template growth method uses sacrificial materials to create pores, however, this approach often confronts challenges in eliminating residual templates and unreacted chemicals.[3–6] Ice crystals are advantageous as porogens, simplifying the template removal process through the freezing of aqueous media and subsequent removal of water by drying, solvent exchange, or lyophilization.[7] The freeze-thaw method stands out as a particularly effective technique for synthesizing porous 3D networks utilizing, ice crystals as porogens. This method promotes the formation of physical entanglements among polymers by concentrating them through the segregation and confinement within frozen solvent crystals.[8] However, the development of porous structures with adequate mechanical durability is contingent upon the choice of polymers, which must be capable of forming robust interactions among themselves. Consequently, the range of polymers suitable for creating porous sponges through simple freeze-thaw cycles is limited. Therefore, there is a critical need to develop versatile methodologies for fabricating sponge materials that extend the range of applicable polymers through the use of eco-friendly freeze-thaw processes. The introduction of cross-linking within a polymer network is a widespread and efficacious strategy to enhance the mechanical and structural stability of porous materials.[9] However, forming cross-links under freezing conditions presents difficulties, as the diffusion of chemicals is significantly reduced and reactivity is diminished in cold and frozen media. Moreover, a complex technique is necessary to manage the simultaneous occurrence of phase separation during the pore-forming step and the cross-linking reaction in the fabrication process. Accordingly,

this study emphasizes the strategic use of thawing steps, typically overlooked in conventional freeze-thaw cycles, expected to address these challenges effectively through post-cross-linking during the gradual thawing phase.

For the fabrication of sponge materials utilizing chitosan as a base material, employing chitosan nanofibers is advantageous because the nanofibers are initially separated from the aqueous media in the solid state. This biphasic condition of the nanofibrous suspension facilitates the formation of porous structures during the freeze-thaw process through a simple phase transition from the aqueous liquid phase to solid ice crystals acting as porogens. This leads to the formation of a chitosan nanofiber-rich phase that forms the structural backbone of the porous material.[10] Consequently, chitosan nanofiber-based sponges are expected to inherit beneficial properties such as a large specific surface area, high porosity, small pore size, and effective channel connectivity.[11]

The demand for fire retardancy (FR) and thermal insulation in polymer design, particularly in sectors such as construction, transportation, and aerospace, has increased significantly.[12,13] While chitosan-based materials are well-recognized for their biomedical applications, they are also being developed for flame-retardant and thermally insulated formulations that minimize environmental impact. Despite chitosan's intrinsic lack of fire-retardant properties, it has been demonstrated that combining chitosan with other polymers and/or flame-retardant additives enhances the fire-retardant behavior of the resultant materials significantly.[14,15] The fire-retardant properties are primarily derived from the role of chitosan as an exceptional carbon source that acts as an effective char-forming material, aiding in the suppression of flame spread. Moreover, the abundant amino groups in chitosan lend themselves to chemical modifications, such as incorporating phosphorus-based flame retardants and cross-linking, which mechanically stabilize the materials. Therefore, the development of chitosan-based sponge materials with robust fire-retardant properties is crucial for advancing towards a sustainable society, offering a preferable alternative to other non-bio-based and non-biodegradable flame-retardant porous materials made from organic and inorganic substances.[16–19]

In this study, a method combining freeze-thaw and post-cross-linking techniques was introduced to develop stable chitosan nanofiber-based sponge materials. Dialdehyde carboxymethyl cellulose (DACMC), an oxidized derivative of carboxymethyl cellulose (CMC), was employed as a cross-linking agent. During the freezing steps of the chitosan nanofiber aqueous suspension, ice crystals

acted as a template for pore generation, inducing phase separation and the formation of a chitosan nanofiber-rich phase. To enhance the physicochemical stability of the porous sponge structure, a cross-linking reaction was conducted by immersing the frozen chitosan nanofiber medium in a dialdehyde carboxymethyl cellulose solution during the thawing step. The gradual diffusion of dialdehyde carboxymethyl cellulose into the thawed sections of the chitosan nanofiber media facilitated the preservation of the porous structure originally templated by ice through cross-linking via ionic interactions and imine bonds, formed between the amino groups of chitosan nanofiber and the carboxyl and aldehyde groups of dialdehyde carboxymethyl cellulose, respectively. This approach also resolves the challenge of polyion complex formation encountered when simply mixing cationic chitosan nanofiber with anionic dialdehyde carboxymethyl cellulose, which impedes the creation of structured porosity through straightforward mixing. The optimal fabrication conditions for the sponge materials were investigated with regard to their mechanical strength, shape recoverability in the wet state and the morphology of the porous structures. Additionally, these materials have been employed for the adsorption of cationic and anionic dyes. The fire-retardant properties under open flame conditions and thermal insulation properties under varying thermal states were also assessed and benchmarked against those of commercially available sponge materials. Given that the synthesis process avoids the use of toxic chemicals and relies on a straightforward methodology using natural-based polymers, this research contributes significantly to the development of eco-friendly approaches for multifunctional sponge materials.

2-2. Experimental Section

Materials and methods

CMC was obtained from Sigma-Aldrich (United States), CSNFs from Sugino Machine Limited (Japan), and hydroxylamine hydrochloride (HAHCl) from Tokyo Chemical Industry Co., Ltd., Japan. Sodium periodate ($NaIO_4$), sodium hydroxide (NaOH), hydrochloric acid (HCl), Congo red (CR), methylene blue (MB), methyl orange (MO), and copper(II) chloride ($CuCl_2$) were sourced from FUJIFILM Wako Pure Chemical Corporation (Japan). All chemicals were used as received.

Oxidation and the characterization of carboxymethyl cellulose (CMC)

CMC was oxidized based on a previously reported procedure with some modifications.[20] An aqueous solution of CMC was prepared by dissolving 10 g CMC in 100 mL distilled water and, adjusting the pH to 3 with 0.1 M HCl. Subsequently, an aqueous solution of $NaIO_4$ was prepared by dissolving 10 g in 100 mL of water and adjusting the pH to 3. Both solutions were then mixed and stirred at 40 °C for 4 h in darkness. Subsequently, the solution was cooled to room temperature, and the oxidized product was precipitated using a large volume of ethanol. The precipitate was collected by vacuum filtration, re-dissolved in water, and dialyzed against distilled water for three days. The final solid product was collected by freeze-drying the dialyzed solution. Dialdehyde carboxymethyl cellulose (DACMC) solutions were prepared by dissolving dry DACMC in phosphate buffer solutions at pH 7.4.

The experimental procedure for determining the DACMC was adapted from previously reported methods, with some modifications.[21] Initially, 0.1 g DACMC was dissolved in 20 mL of an aqueous solution, and the pH was adjusted to 5 using 1 M NaOH. A 25 mL solution of HAHCl at a concentration of 0.25 M, adjusted to pH 5, was prepared. The solutions were mixed and stirred at 40 °C for 4 h. Subsequently, the mixtures were titrated back to the initial pH of 5 using a 0.1 M NaOH solution. This experiment was conducted in triplicate.

The aldehyde content (*AC*) was calculated using the equation (1)

$$AC = \frac{C_{NaOH} * V_{NaOH}}{m_{DACMC}} \quad (1)$$

C is the NaOH concentration, *V* is the NaOH volume, and *m* is the weight of DACMC.

Preparation and optimization of the CSNFs-DACMC composite

Initially, an aqueous suspension of chitosan nanofibers (CSNFs) was prepared. Acetic acid was added dropwise to the suspension, which was then stirred continuously overnight. The pH was adjusted to approximately 6.3 using this procedure. The concentration of CSNFs was varied at 1%, 1.5%, 2%, 2.5%, and 3 wt% to determine the optimal concentration. Subsequently, 2 mL of each concentration were dispensed into small glass vials and subjected to freezing at temperatures of -40 °C, -25 °C, and -10 °C. These samples were maintained at these temperatures for 12 hours. An excess of dialdehyde carboxymethyl cellulose (DACMC) (5.0 wt%) was then introduced to the

samples. Following the addition of dialdehyde carboxymethyl cellulose, thawing cycles were initiated, with samples maintained at 4 °C, 10 °C, and 25 °C for 12 hours per cycle. This freeze-thaw process was repeated five times. Finally, the samples were rinsed with deionized water to remove any unreacted dialdehyde carboxymethyl cellulose and were termed CSNF-DACMC composites. For drying, samples were frozen in liquid nitrogen and then lyophilized.

Characterization of the samples

Material characterization was performed using attenuated total reflection-Fourier transform infrared (ATR-FTIR) spectroscopy (Thermo Scientific Nicolet iS5 equipped with an iD5 ATR attachment, United States), with scans conducted over a wavenumber range from 4000 to 500 cm^{-1}. The samples were frozen using liquid nitrogen and lyophilized in a vacuum freeze drier. The micromorphologies of the samples were examined using scanning electron microscopy (SEM) (Hitachi SU3500, Japan). For SEM analysis, lyophilized samples were coated with gold-palladium using an MSP-1S magnetron sputter (Vacuum Device Inc., Japan) and observed in high-vacuum mode at an acceleration voltage of 1.50 kV.

The density (d), water adsorption capacity, and porosity of the samples were analyzed using equations 2, 3, and 4, respectively:

$$d = \frac{W_d}{v}, \tag{2}$$

where W_d is the dry weight, and v is the volume, which was calculated by considering the material as a cylinder.

$$Water\ adsorption\ capacity\ = \frac{W_w - W_d}{W_d}\ 100 \tag{3}$$

where W_w is the wet weight obtained by simply removing the surface water, and W_d is the dry weight.

Porosity was evaluated using a method previously reported in the literature.[22] Initially, the volume (V) of the cylindrical sponge was determined. The initial dry weight (W_0) of each sample was recorded. Subsequently, the samples were immersed in 99 wt% ethanol at a temperature of 25 °C for 24 hours. After immersion, the final weight (W_1) of each sample was measured. The density of ethanol (ρ) was also considered in these calculations.

$$Porosity = \frac{W_1 - W_0}{\rho V} 100 \quad (4)$$

Mechanical strength of the samples

The mechanical strength of both dry and wet samples was assessed separately. For wet samples, a 50 N load cell was employed, and compression tests were conducted at a rate of 3.0 mm/min using a universal testing machine (UTM) (Shimadzu EZ Graph, Japan). Cyclic compression tests for wet samples involved varying the strain to 20%, 40%, 60%, and 80%. The durability of these samples was determined based on the stress values at 80% strain during 20 compression cycles.

For completely dried samples, linear compression was performed at a rate of 3 mm min^{-1} using a 500 N load cell.

Determination of thermal insulation and fire retardancy

A composite sample fabricated under specific conditions, frozen temperature of -25 °C, thawing temperature of 4 °C, 2.5 wt% chitosan nanofibers (CSNFs) concentration, and 5 wt% dialdehyde carboxymethyl cellulose (DACMC) concentration was utilized to evaluate thermal insulation and fire retardancy properties. Initially, thermal insulation properties were assessed using infrared thermography (FLIR, Sweden). A setup involving a hot plate maintained at 100 °C and a cool plate at -6 °C was established, with the dried CSNFs-DACMC composite placed between them, covered by a thin glass slide. Infrared (IR) images were captured at 1-minute intervals for 30 minutes and subsequently at 10-minute intervals for an additional hour to monitor the temperature on the material's surface. This behavior was benchmarked against commercially available sponges made from cellulose, polyurethane (PU), and polystyrene (PS). Fire retardancy was evaluated by subjecting the materials to an open flame. Parameters such as flame spreading rate, char formation rate, and ignition time were recorded by burning samples with dimensions of 2 cm in length and 2 mm in thickness. The performance was compared with that of commercially available foams. Three replicates were used for this testing, and the average values were calculated.

Evaluation of dye adsorption behavior

To evaluate adsorption properties, aqueous solutions of Congo red (CR), methylene blue (MB), and methyl orange (MO) were prepared at a concentration of 10 mg/L. The composite samples were immersed in these solutions and agitated at 25 °C for 24 hours. Post-treatment, the UV

absorbance of the solutions was measured at 498 nm for CR, 664 nm for MB, and 464 nm for MO. The amount of dye adsorbed by the samples was quantified using calibration curves.

2-3. Results and Discussion

The CSNF-DACMC composite sponge materials were developed using an integrated freeze-thaw method and a cross-linking reaction during the thawing stages. The design and fabrication strategy of the sponge materials are depicted in **Figure 2-1a**. The composite utilizes sustainable polysaccharides, with chitosan nanofibers (CSNFs) serving as the primary structural component and dialdehyde carboxymethyl cellulose (DACMC) functioning as the crosslinker. The chitosan nanofibers, commercially produced through aqueous counter-collision methods, demonstrated a high aspect ratio, with lengths in the hundreds of micrometers and a diameter of approximately 160 nm. dialdehyde carboxymethyl cellulose, synthesized via the oxidation of carboxymethyl cellulose, acted as an effective cross-linking agent due to its carboxyl and aldehyde groups, which facilitated the formation of ionic interactions and imine bonds with the amino groups of chitosan nanofibers (**Figure 2-1b**). The fabrication process began with the freezing of an aqueous chitosan nanofiber dispersion. This freeze-thaw cycle promoted template growth, where ice crystals served as a template for the porous network (**Figure 2-1a**). The freezing of the aqueous suspension led to the formation of concentrated chitosan nanofiber domains adjacent to the ice crystals.[23] Subsequently, the frozen chitosan nanofiber medium was immersed in a dialdehyde carboxymethyl cellulose aqueous solution at a carefully controlled thawing temperature. As the ice melted gradually during the thawing stage, dialdehyde carboxymethyl cellulose was integrated into the 3D structure of the chitosan nanofiber domains, reinforcing the material through cross-linking between chitosan nanofiber and dialdehyde carboxymethyl cellulose via ionic interactions, imine bonds, and hydrogen bonds. The diffusion of dialdehyde carboxymethyl cellulose from the surface of the melting ice allowed for the maintenance of the 3D structure and shape of the materials, ensuring structural integrity even after the ice template had melted away. Repeated freeze-thaw cycles further solidified the stability of physical interactions.

The CSNF-DACMC wet sponge materials were successfully fabricated after undergoing five freeze-thaw cycles, as depicted in **Figure 2-2a** and **b**. These composites demonstrated exceptional shape recoverability in their wet state, able to return to their original form upon the release of compressive stress, as shown in **Figure 2-2c**. This resilience was evident during compression tests conducted in axial and parallel directions, confirming the homogeneity and stability of the network. Subsequently, the wet sponges were lyophilized to obtain dried porous materials, which displayed a remarkably low specific density. The structural integrity was such that even thin flowers and stems could support the weight of the material, as illustrated in **Figure 2-2b**.

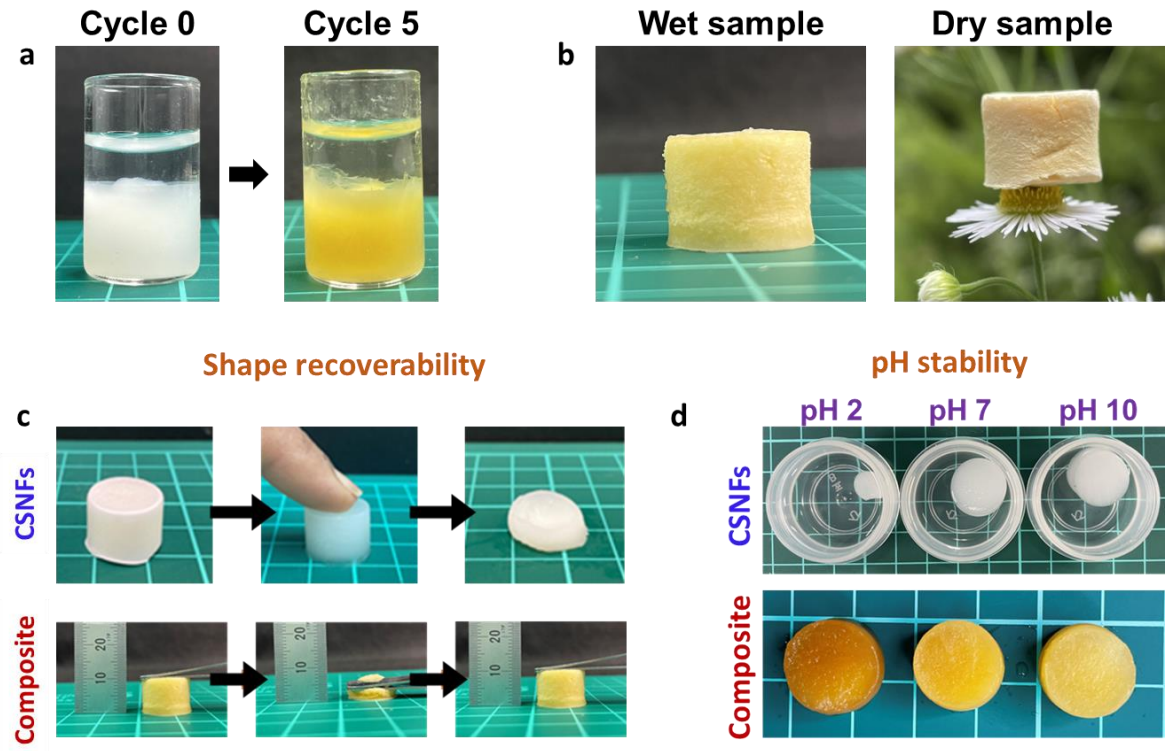

Figure 2-2. Photographs of the CSNFs-DACMC composite (a) before start the FT cycles and after completing five FT cycles. (b) in wet state and dry states. (c) demonstrating the shape recoverability of the wet sample compared to the CSNFs-made foam. (d) demonstrating the pH stability compared to the CSNFs-made foam.

In a control experiment to evaluate the effect of composite formation, a sample consisting solely of chitosan nanofibers (CSNFs) (CSNFs foam) was prepared. This sample was fabricated by freezing the CSNFs aqueous media omitting the dialdehyde carboxymethyl cellulose (DACMC) solution during the thawing step, and directing it to lyophilization after freezing. Unlike the CSNF-

DACMC composite, the chitosan nanofiber foam exhibited no shape recovery behavior in water and was completely deformed after compression (**Figure 2-2c**).

Additionally, a sample comprised only of dialdehyde carboxymethyl cellulose (DACMC) (DACMC foam) was prepared by freezing and lyophilizing the DACMC aqueous solution. This sample disintegrated in water shortly after immersion. These observations underscore the crucial role of DACMC in enhancing the stability of the composite through cross-linking with chitosan nanofibers and highlight the importance of the cross-linked 3D structure for the functional behavior of the sponge.

Chitosan (CS) is recognized for its solubility in acidic solutions, a property attributed to the protonation of its primary amino groups under acidic conditions. While this characteristic can be advantageous, it poses challenges regarding the pH stability of CS-based materials for certain applications. In a comparative analysis, the chitosan nanofibers (CSNFs) foam, without the cross-linking and robust 3D structure of the composite, was unable to maintain its shape under the same acidic condition and disintegrated rapidly while the CSNFs-DACMC composite material was stable in all the pH conditions with a slight swelling in pH 2 aqueous solution but still maintain its structure despite deformation. (**Figure 2-2d)**. These findings underscore the critical importance of a cross-linked 3D structure for maintaining the stability and functionality of chitosan-based sponges across a broad range of pH conditions. This structural integrity ensures that the composite materials can withstand various environmental stresses, making them suitable for diverse applications where pH fluctuations might otherwise compromise material performance.

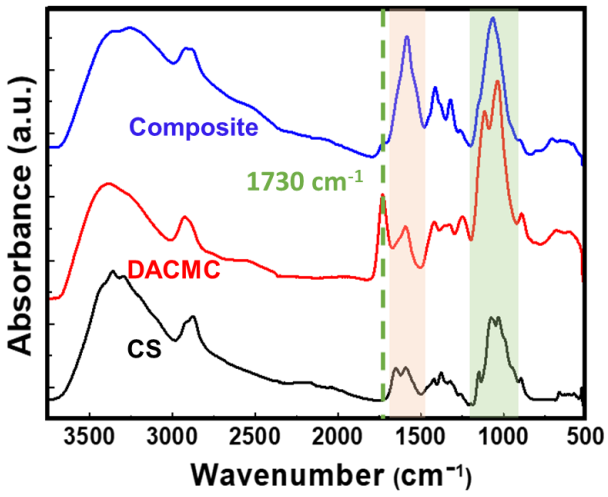

Figure 2-3. FTIR spectra of CSNFs, DACMC, and CSNFs-DACMC composite.

Fourier transform infrared (FTIR) spectroscopy was performed to characterize the chemical bonding within the materials (**Figure. 2-3**). For dialdehyde carboxymethyl cellulose (DACMC), a peak at 1590 cm^{-1} corresponding to the C=O stretching vibration of the carboxylate group was also observed in carboxymethyl cellulose (CMC). Additionally, a distinct peak at 1730 cm^{-1} in DACMC was

identified as the C=O stretching vibration of the aldehyde group, indicative of the successful oxidation reaction facilitated by $NaIO_4$. The modification ratio of the aldehyde group was determined to be 6.5±0.1 mmol/g, the peak at 1500 cm^{-1} was associated with the N-H bending vibration of the amide group and another at 1600 cm^{-1} with the C=O stretching of the amide group. Notably, in the CSNF-DACMC composites, the prominent aldehyde peak of dialdehyde carboxymethyl cellulose (DACMC) at 1730 cm^{-1} was decreased, signaling the successful formation of imine bonds. This observation corroborates the cross-linking via imine bonds between the aldehyde groups in DACMC and the amino groups in CSNFs within the composite materials, enhancing their structural and functional properties.

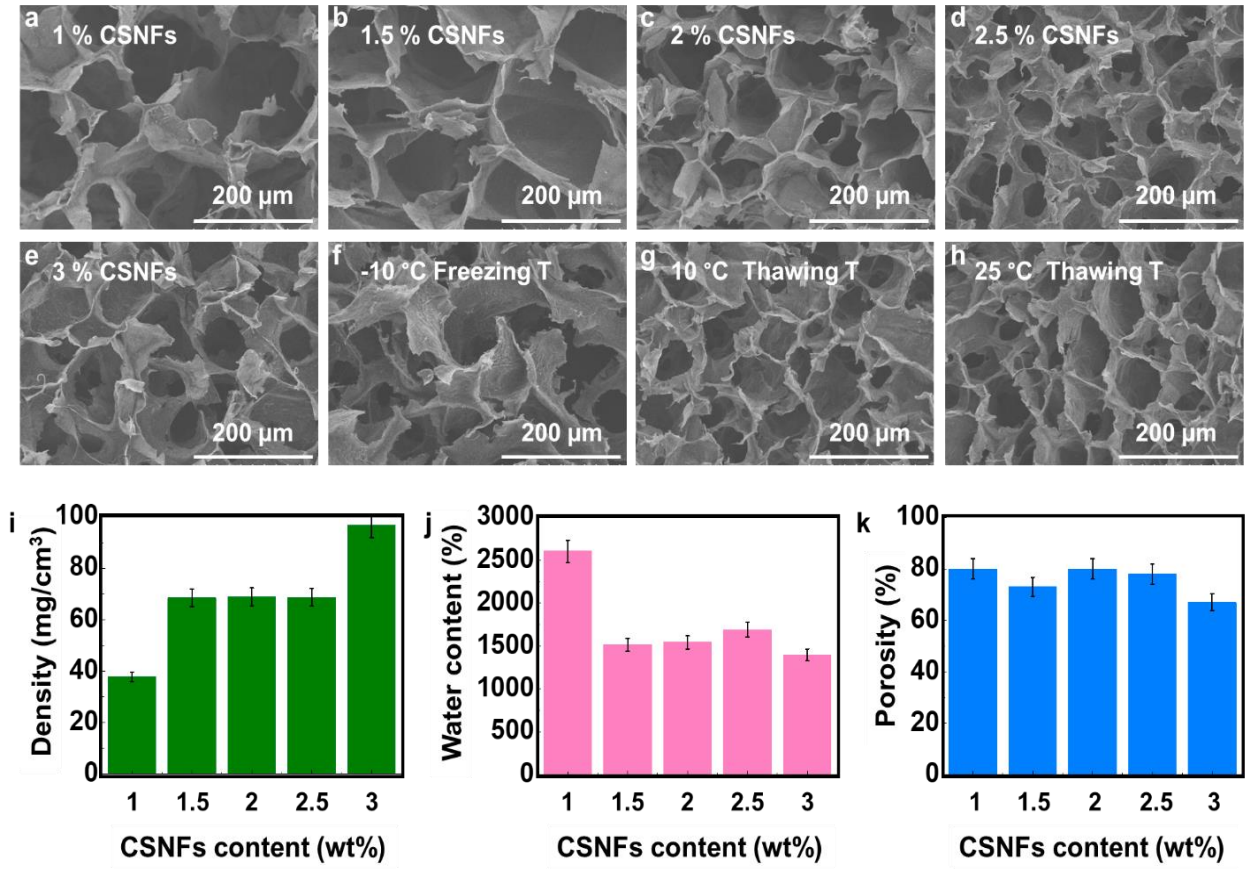

Figure 2-4. SEM images of CSNFs-DACMC composites with varying CSNF concentrations (1%, 1.5%, 2%, 2.5%, and 3%), frozen at -25 °C and thawed at 4 °C shown in (a-e). SEM image of the composite with 2.5 wt% CSNFs frozen at (f) -10 °C, (g) -25 °C and thawed at 10 °C, and (h) -25 °C and thawed at 25 °C. Plots depicting (i) density, (j) water content, and (k) porosity of the composites as functions of CSNF concentration.

The internal morphologies of the samples were examined using SEM. The composite showcased a honeycomb-like porous structure, attributed to the random freezing of water and the aggregation of chitosan nanofibers (CSNF). Importantly, the porous structure of the CSNF-DACMC composite was comparable to that of the CSNFs foam, indicating that the porous morphology was primarily established during the freezing process of the CSNFs media. The pore size varied depending on the synthesis conditions. Specifically, the pore size decreased from approximately 130 μm to 70 μm when the CSNF concentration was increased from 1.0 to 3.0 wt% (**Figure 2-4a-e**). This variation in pore size is mainly due to the change in ice crystal size during the freezing step; higher concentrations of CSNFs resulted in smaller ice crystals, as the presence of a larger number of fibrous polymer domains led to a separation into ice-rich and polymer-rich phases. Furthermore, the mobility of the fibers within the media was restricted at higher viscosities and chitosan nanofiber (CSNF) concentrations, resulting in the formation of smaller ice crystals. Additionally, variations in freezing and thawing temperatures were explored. The pore size of the composite prepared at a freezing temperature of -10 °C was larger compared to that at -25 °C (**Figure 2-4d,** and **f**). This difference is attributed to the fact that lower freezing temperatures result in faster freezing rates, thereby producing smaller ice crystals. These findings demonstrate that pore size can be adjusted by modifying the synthesis conditions. However, SEM images indicated that the thawing temperature did not significantly affect the pore size (**Figure 2-4g,** and **h**).

The fundamental properties of the CSNF-DACMC sponge, such as density, water absorbency, and porosity, were thoroughly investigated. The density of the composite increased with chitosan nanofiber (CSNF) concentration, with the sample containing 2.5 wt% CSNFs exhibiting a density of approximately 70 mg/cm^3 (**Figure 2-4i**). The densities of most samples remained below 100 mg/cm^3, classifying the sponge materials as lightweight. Water content, calculated based on the ratio of water to the dry weight of the composite, was approximately 1500%, except for the sample with 1.0 wt% CSNFs, which demonstrated outstanding water absorbency (**Figure 2-4j**). Moreover, nearly all samples exhibited more than 70% porosity (**Figure 2-4k**). From these results, it is evident that the CSNF-DACMC composite displays key characteristics of sponge materials, such as high porosity and excellent water absorbency, facilitated by its continuous honeycomb-like porous structure.

The mechanical properties of both wet and dry CSNF-DACMC composites were comprehensively evaluated. The dry samples displayed characteristics typical of an aerogel, which involved three distinct stages: initial low-strain linear elastic behavior, a yield area with a reduced slope, and a high-strain dense area. Notably, the mechanical properties such as Young's modulus were found to increase with the concentration of CSNFs (**Figure 2-5a,** and **b**). The sample

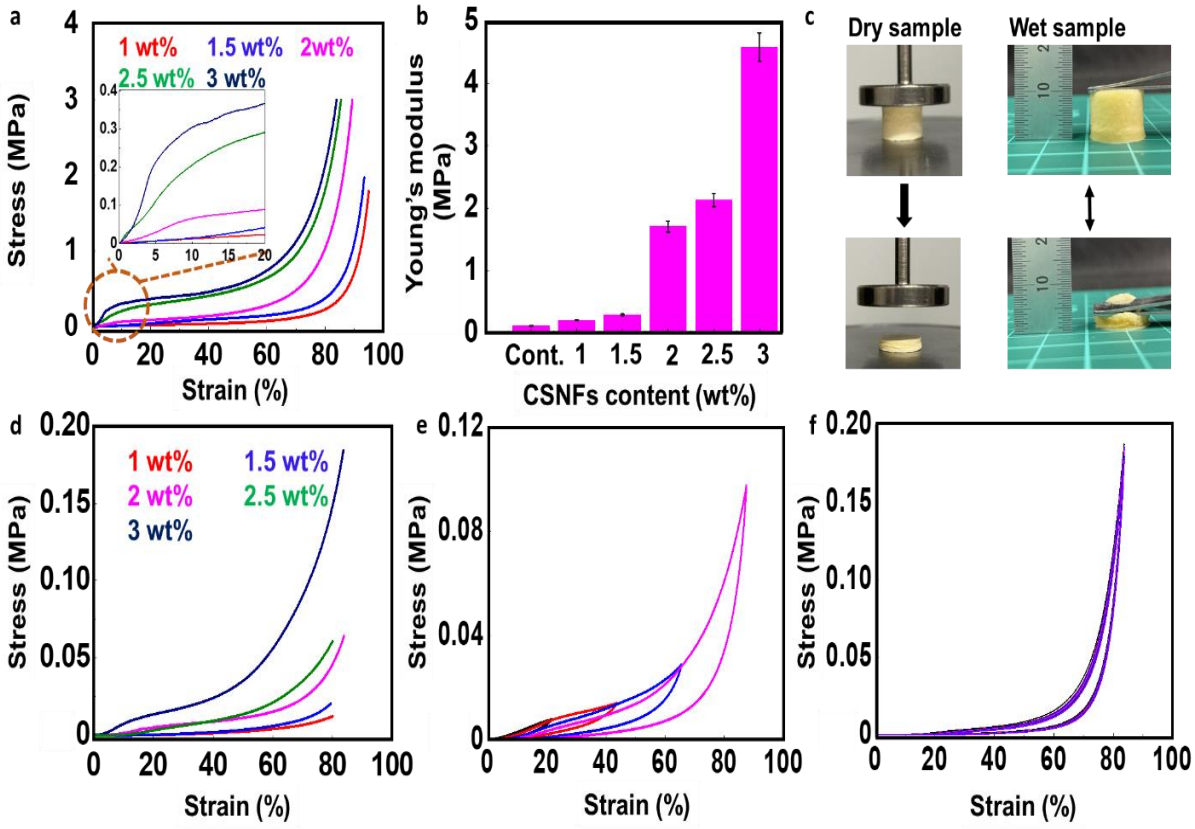

Figure 2-5. (a) Compression stress-strain curves for the dry CSNFs-DACMC composite. (b) Young's modulus of the dry composite across various CSNF concentrations. (c) Images showcasing shape recoverability comparing dry and wet states. (d) Compression stress-strain curves for the wet composite. (e-f) Cyclic compression stress-strain curves for the wet composite under different and constant strains, respectively, using samples with 2.5 wt% CSNFs frozen at -25 ℃ and thawed at 4 ℃.

containing 3.0 wt% CSNFs, however, was brittle and fractured easily under compression. In contrast, the other samples could be compressed into thin discs without breaking (**Figure. 2-5c**), and notably, these samples swelled back to their original cylindrical shape upon immersion in water, demonstrating significant recoverability.

For the wet samples, mechanical strength also increased with chitosan nanofiber (CSNF) concentration (**Figure. 2-5d**). These samples exhibited repeated compressibility and the ability to recover to their initial state across all strain percentages (**Figure. 2-5e,** and **f**), which is characteristic of sponge materials. The mechanical strength notably increased with CSNF concentration. Samples with 2.5 and 2 wt% CSNFs exhibited smaller reductions in compression stress after successive cycles of compression and release compared to other samples. Optimal parameters were identified as 2.5 wt% CSNFs, a freezing temperature of -25 ℃, and a thawing temperature of 4 °C, based on the observed energy dissipation behavior.

Additionally, the inherent primary amino groups of chitosan and the carboxylic groups of dialdehyde carboxymethyl cellulose (DACMC) endow the materials with the capability to adsorb anionic and cationic materials.[24,25] Congo red was utilized to assess the adsorption behavior of CSNF-DACMC at a pH of 6.7. The material was able to adsorb approximately 98% of the dye from the solution (**Figure 2-6a**), with an adsorption capacity of 4.8×10^2 mg/g for Congo red. This high adsorption capacity primarily arises from the interactions between the cationic amino groups of the chitosan nanofibers (CSNFs) and the sulfate anion of Congo red. An adsorption experiment using cationic methylene blue demonstrated that approximately 90% of methylene blue was adsorbed at pH 10.2 (**Figure 2-6b**), with an adsorption capacity of 67 mg/g. The primary mechanism for the adsorption of cationic methylene blue is attributed to electrostatic interactions with the anionic carboxylate groups of DACMC. In the case of the anionic dye methyl orange,

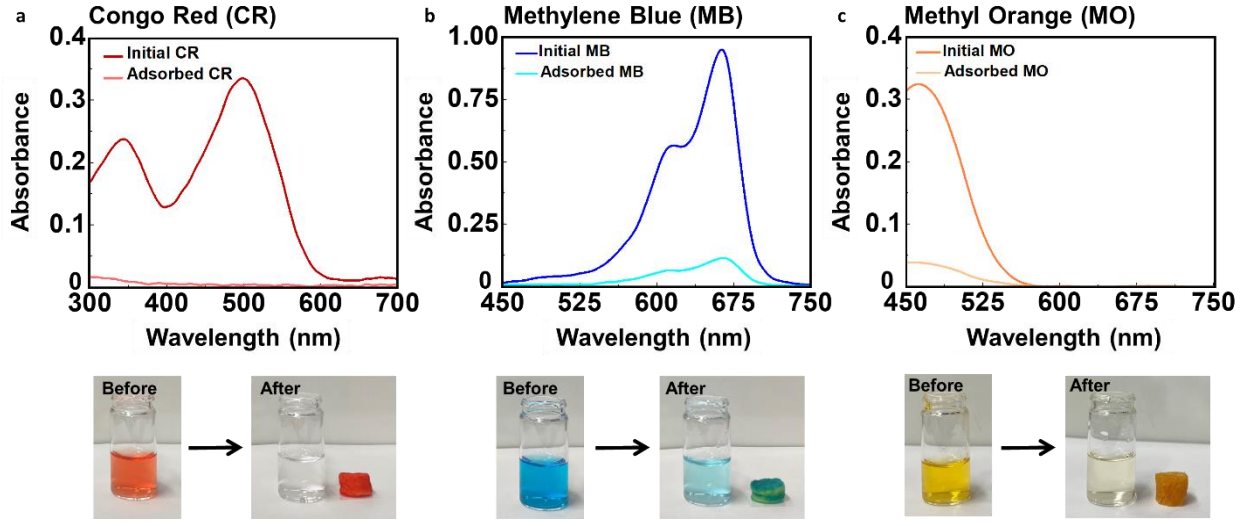

Figure 2-6. UV spectra and photographs of dye solutions (a) CR, (b) MB, and (c) MO before and after adsorption by the CSNFs-DACMC composite (2.5 wt%, FT -25 ℃, TT 4 ℃).

approximately 85% of the dye was adsorbed by the sample at pH 6.8, with an adsorption capacity of 56 mg/g (**Figure 2-6c**). These results underscore the composite's utility for adsorbing both anionic and cationic dyes.

The fire-retardant properties of the CSNF-DACMC sponge materials were also evaluated. When exposed to an open flame, the CSNF-DACMC did not ignite. The material demonstrated self-extinguishing properties, as the flame did not propagate further and was extinguished immediately upon removal from the flame. This behavior contrasts starkly with that observed in commercially available cellulose, polystyrene, and polyurethane foams (**Figure 2-7a, b, c,** and **d**), which burned completely, leaving only ash. The fire-retardant properties, such as ignition time, flame transfer rate, and char formation rate, were further investigated. While the edges of the cellulose, polystyrene, and polyuratahne foams ignited rapidly, allowing the flame to spread quickly to the other side of the materials and resulting in complete combustion the CSNF-DACMC sponge did not ignite and ceased burning upon removal from the flame, gradually forming a stable char layer. This resulted in a low char formation rate of 0.16 cm/s, as the formation of a protective char layer significantly hindered the spread of flames across the material's surface.

Figure 2-7. Photographs demonstrating the behavior under open flame of (a) CSNFs-DACMC (2.5 wt%, FT -25 ˚C, TT 4 °C), and commercial (b) cellulose, (c) PU, and (d) PS foams.

Following exposure to fire, the burned samples, including chitosan nanofiber (CSNF) foam, dialdehyde carboxymethyl cellulose (DACMC) foam, and CSNF-DACMC composite sponges, were analyzed to assess the components contributing to their remarkable fire-retardant behavior. The fire retardancy mechanisms of these materials can be categorized into two types. The first is intumescent fire-retardant behavior, where the material swells upon degradation and forms a

porous foam structure, creating an effective barrier against heat, air, and pyrolysis products. The second mechanism involves char formation, where the material develops a dense and stable carbonaceous layer on its surface, blocking the diffusion of gaseous products to the flame and thereby shielding the underlying material from heat.[13] For the chitosan nanofiber (CSNFs) foam, upon exposure to fire, it contracted and formed a char layer on the burned surface (**Figure 2-8a**). Despite the formation of dense structures within the char layers, a porous morphology was still discernible in the SEM images. The chitosan nanofiber displayed slight ignition, but the fire quickly extinguished. The dialdehyde carboxymethyl cellulose (DACMC) foam primarily exhibited intumescent behavior. **Figure 2-8b** illustrates the swelling behavior of DACMC foam upon contact with the flame, resulting in an ash-like, fluffy, and unstable layer atop the sample. SEM images of the burned section revealed a slightly porous structure characteristic of intumescent fire retardancy. In contrast, the CSNF-DACMC composite sponge neither swelled significantly nor contracted dramatically upon exposure to flame but showed behavior akin to that of the chitosan nanofiber foam (**Figure 2-8c**). The char formed by the CSNF-DACMC sponge produced a continuous, layer-like structure that effectively covered and protected the lower parts of the sponge not directly in contact with the fire. Furthermore, when control samples of CSNF-DACMC films were subjected to an open flame, both film samples displayed slight ignition, with flame distribution. These observations suggest that the integration of CSNFs and DACMC

enhances the char formation and stability, contributing significantly to the fire-retardant properties of the composite material.

The DACMC films demonstrated notable intumescent behavior upon exposure to fire, effectively swelling to form a protective layer. In the case of CSNF films, the spread of flame across the material was effectively suppressed due to the ability of CS to serve as an excellent carbon source for stable char layer formation, thereby enhancing its FR properties. Compared to individual films, the CSNF-DACMC composites exhibited enhanced FR properties, such as greater shape stability and a self-extinguishing nature. These results underscore that the CSNF-

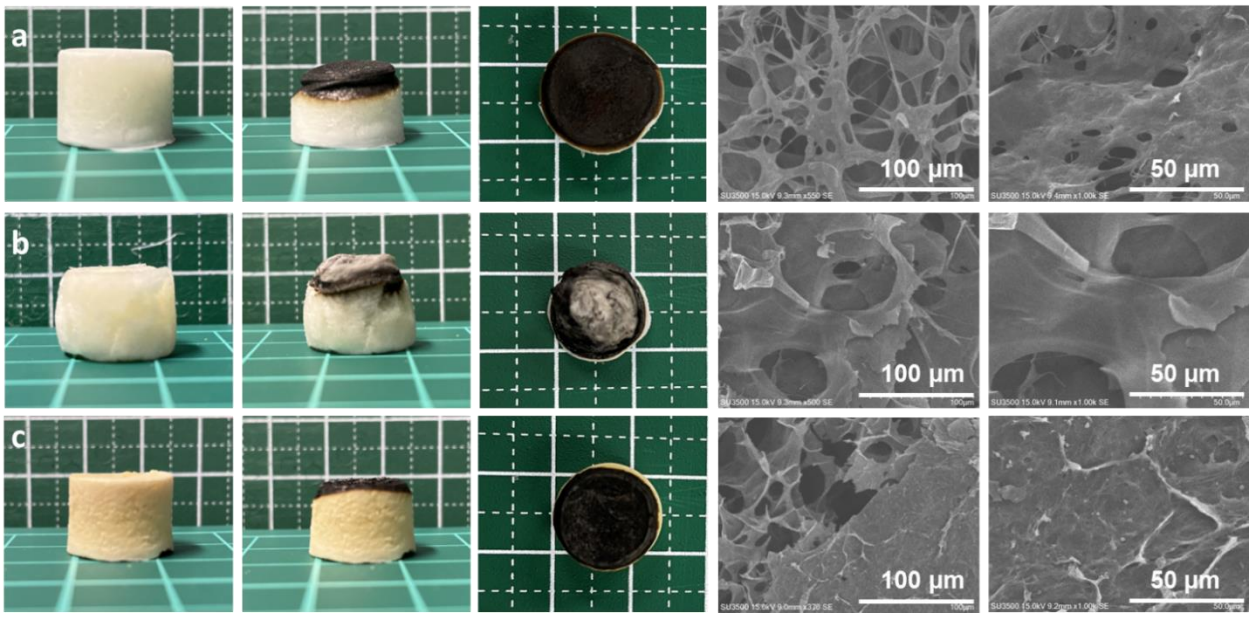

Figure 2-8. Photographs and SEM images of the char layer formation on (a) CSNFs, (b) DACMC foams, and (c) CSNFs-DACMC (2.5 wt%, FT -25 °C, TT 4 °C) after exposure to open flame.

DACMC sponge materials display exceptional FR behavior due to their strong mechanical

properties, which are derived from compositing with cross-linking and a porous morphology that facilitates the formation of a stable char layer.

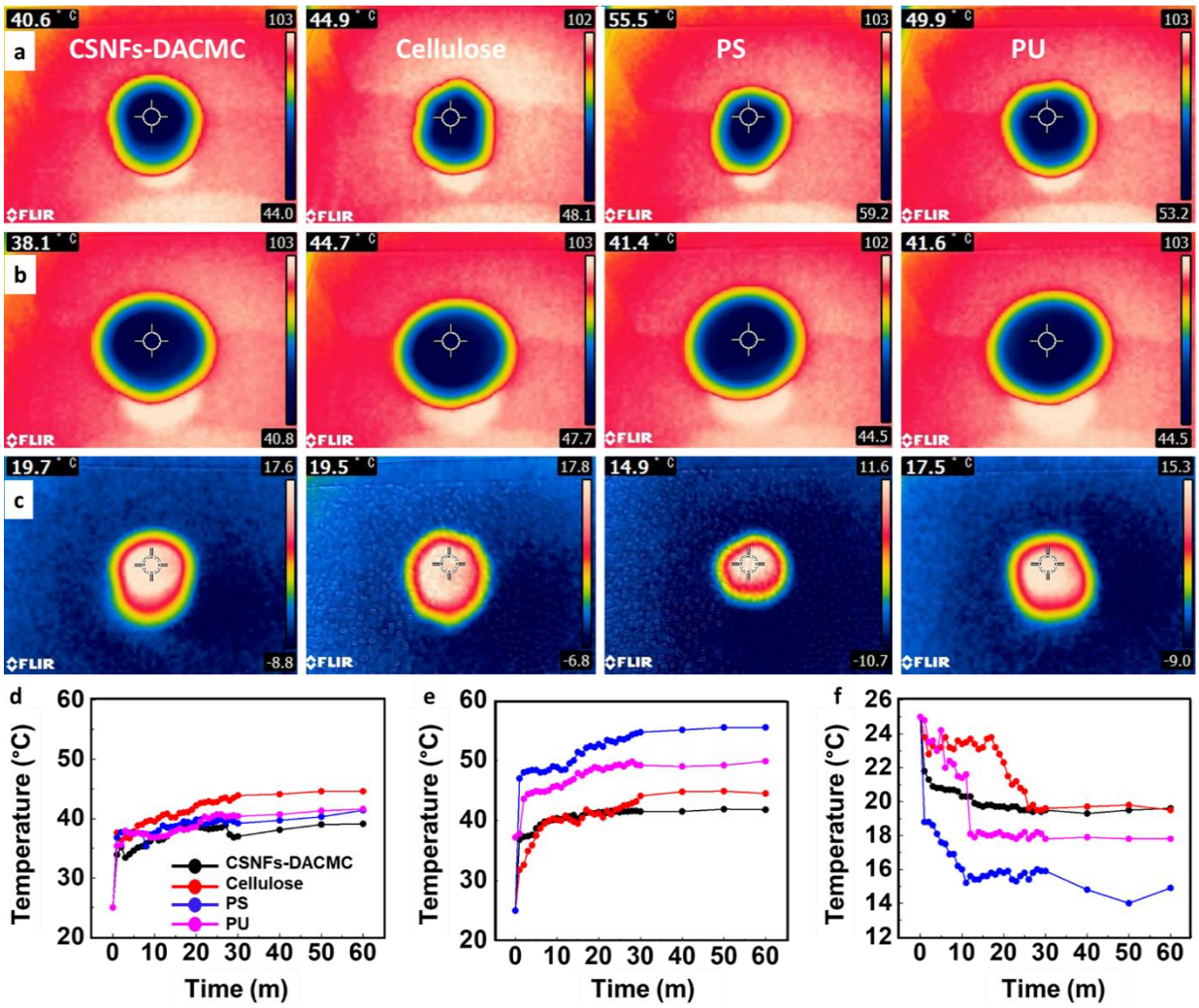

Figure 2-9. (a, d) IR images and time-to-temperature graphs for CSNFs-DACMC and commercial foams on a hot plate at 100 ºC for 1 hour. (b, e) IR images and time-to-temperature graphs for CSNFs-DACMC and commercial foams on a hot plate at 100 ºC with a glass plate on top for 1 hour. (c, f) IR images and time-to-temperature graphs for CSNFs-DACMC and commercial foams on a cold plate at -10 ºC.

Subsequently, the thermal insulation behavior of the CSNF-DACMC dry sponge was investigated. The sample was placed on a hot plate set at 100 ℃ and thermal behavior was monitored using an IR thermographic camera. The temperatures of the heated sample surfaces and the glass plates positioned above them were individually recorded. Similar examinations were

conducted with cellulose, PS, and PU foams. The results revealed that the thermal insulation performance of the CSNF-DACMC composite surpassed that of the other commercial materials (**Figure 2-9**). The composite maintained a temperature of around 40 ℃ even after 1 hour (**Figure 2-9a** and **d**). Additionally, when a glass plate was placed atop the sample, the temperature remained around 38 ℃ after 1 hour (**Figure 2-9b** and **e**). When positioned on a cold plate, the temperature did not drop below 19 ℃ (**Figure 2-9c** and **f**), indicating robust thermal insulation in both hot and cold environments. The composite's porous structure significantly contributes to this thermal insulation by impeding thermal convection. Furthermore, the 3D network acts as a thermal barrier by creating a complex path that hinders the transfer of heat waves. When the composite was placed on a hand and observed with an IR camera, it effectively blocked the thermal IR radiation emitted by the human body. This characteristic suggests potential applications for the composite as an infrared camouflage material, utilizing its unique properties to enhance both safety and efficiency in various applications.

2-4. Conclusions

Sponge materials comprising biomass resources, specifically CSNFs and DACMC, were successfully synthesized using a freeze-thaw method complemented by post-cross-linking during the thawing phase. CSNF-rich phases were cross-linked by subsequent thawing facilitating the gradual diffusion of DACMC from the thawed CSNFs medium, enabling the formation of stable porous structures through ionic interactions and imine bonds. The optimal parameters for fabrication were identified as 2.5 wt% CSNFs and 5 wt% DACMC, with a freezing temperature of -25 °C and a thawing temperature of 4 °C. Under wet conditions, the material functioned effectively as a sponge, demonstrating exceptional shape recoverability. The CSNF-DACMC composite proved to be an effective adsorbent for both anionic and cationic dyes, utilizing the cationic nature of CS's amino groups and the anionic properties of DACMC's carboxylic acid groups. In its dry state, the CSNF-DACMC composite exhibited properties akin to those of an aerogel, serving as an excellent thermal insulator by creating a complex pathway that impedes heat transfer in diverse thermal environments. Its insulation performance surpassed that of conventional commercial materials such as PS and PU foams. Moreover, the composite demonstrated

outstanding fire-retardant properties by forming a stable char layer that effectively hindered combustion. The synthesis process, free from toxic chemicals and relying on natural-based polymers, represents a significant advancement in the development of eco-friendly methods for fabricating multifunctional materials. This study not only demonstrates the potential of CSNF-DACMC composites in various applications but also emphasizes the environmental benefits of using sustainable resources in material engineering.

2-5. References

(1) H. Kargarzadeh, J. Huang, N. Lin, I. Ahmad, M. Mariano, A. Dufresne, S. Thomas, A. Gałęski, *Prog. Polym. Sci.* **2018**, *87*, 197.

(2) A. M. Usmani, I.O. Salyer, *Polym. Plast. Technol. Eng.* **1979**, *12*, 61.

(3) Y. E. Shin, Y. J. Sa, S. Park, J. Lee, K.H. Shin, S. H. Joo, H. Ko, *Nanoscale* **2014**, *6*, 9734.

(4) R. Starbird, C. A. García-González, I. Smirnova, W. H. Krautschneider, W. Bauhofer, *Mater. Sci. Eng. C Mater. Biol. Appl.* **2014**, *37*, 177.

(5) Y. Wang, J. Zhang, S. Chen, X. Zhang, Y. Li, Z. Yang, *ACS Appl. Polym. Mater.* **2023**, *5*, 2490.

(6) G. Duan, S. Jiang, T. Moss, S Agarwal, A. Greiner, *Polym. Chem.* **2016**, *7*, 2759.

(7) H. Takase, K. Shiomori, Y. Okamoto, N. Watanabe, H. Matsune, H. Umakoshi, *ACS Appl. Polym. Mater.* **2022**, *4*, 7081.

(8) L. Zhang, Y. Wang, C. Chang, *Macromol. Mater. Eng.* **2010**, *295*, 137.

(9) S. A. Bernal-Chávez, A. Romero-Montero, H. Hernández-Parra, S. I. Peña-Corona, M. L. Del Prado-Audelo, S. Alcalá-Alcalá, H. Cortés, L. Kiyekbayeva, J. Sharifi-Rad, G. Leyva-Gómez, *J. Biol. Eng.* **2023**, *17,* 35.

(10) D. Zong, X. Zhang, X. Yin, F. Wang, J. Yu, S. Zhang, B. Ding, *Adv. Fiber Mater.* **2022**, *4*, 1434.

(11) P. Risch, C. A. Adlhart, *ACS Appl. Polym. Mater.* **2021**, *3*, 4685.

(12) C. Liu, S. Wu, Z. Yang, H. Sun, Z. Zhu, W. Liang, A. Li, *ACS Omega* **2020**, *5*, 8638.

(13) B. W. Liu, H. B. Zhao, Y. Z. Wang, *Adv. Mater.* **2022**, *34,* 2107905.

(14) H. He, Y. Wang, Z. Yu, J. Liu, Y. Zhao, Y. Ke, *Carbohydr. Polym.* **2021**, *269*, 118291.

(15) G. Malucelli, *Molecules* **2020**, *25*, 4046.

(16) S. Zhang, X. Liu, X. Jin, H. Li, J. Sun, X. Gu, *Carbohydr. Polym.* **2018**, *189*, 313.

(17) H. Yu, X. Xu, Y. Xia, M. Pan, N. Zarshad, B. Pang, A. U. Rahman, M. Wu, H. Ni, *E-Polymers* **2020**, *20*, 303.

(18) G. Makhlouf, A. Abdelkhalik, H. Ameen, *Prog. Org. Coat.* **2022**, *163*, 106627.

(19) F. Carosio, M. Ghanadpour, J. Alongi, L. Wågberg, *Carbohydr. Polym.* **2018**, *202*, 479.

(20) H. Li, B. Wu, C. Mu, W. Lin, *Carbohydr. Polym.* **2011**, *84*, 881.

(21) Y. Yi, Z. Jiang, S. Yang, W. Ding, Y. Wang, B. Shi, *Carbohydr. Polym.* **2020**, *239*, 116217.

(22) X. Yang, D. Yang, X. Lin, D. Li, W. Shi, Z. Xiang, C. Mu, L. Ge, D. Li, Z. Xu, *ACS Appl. Polym. Mater.* **2023**, *5*, 3427.

(23) M. Zhang, S. Jiang, F. Han, M. Li, N. Wang, L. Liu, *Carbohydr. Polym.* **2021**, *264*,118033.

(24) M. Wang, Y. Ma, Y. Sun, S. Y. Hong, S. K. Lee, B. Yoon, L. Chen, L. Ci, J. Nam-Do; X. Chen, J. Suhr, *Sci. Rep.* **2017**, *7*, 18054.

(25) E. N. Mohamed, A. I. Abd-Elhamid, A. A. El-Bardan, H. M. A. Soliman, M. S. Mohy-Eldin, *Sci. Rep.* **2023**, *13,* 14265.

Chapter 3

Clusterization-Triggered Emission of Polysaccharide-based Microclusters induced by the Co-assembly of Chitosan Nanofibers and Dialdehyde Carboxymethyl Cellulose

3-1. Introduction

The use of luminescent materials has drastically increased in many areas such as information storage, sensors, cell imaging, and photoelectronic devices. Conventional luminogens that rely on through-bond conjugations (TBC) via extended π-electronic structures are currently being developed and used in many applications owing to their high emission efficiency and tunable color. However, conventional luminogens have several drawbacks, such as synthetic complications, poor water solubility, and inevitable toxicity. Moreover, most of these materials exhibit aggregation-caused quenching at high concentrations.[1–3] These challenges limit their practical applications. In contrast, some natural polymers that emit in the aggregated state provide solutions to the above-mentioned problems associated with conventional luminogens because of their low toxicity, good processability, and biocompatibility. The concept of non-conventional luminophores was first proposed in 1605 by Francis Bacon, who observed luminescence in sugar. Research interest in this unique luminescent behavior has increased in recent years. These non-conventional luminophores are non-conjugated systems with abundant electron-rich heteroatoms such as nitrogen, oxygen, phosphorous, and sulfur or functional groups like C=O, C=C, C=N, and C≡N. They fluoresce mostly in the clusterized state at high concentrations and in the solid state, whereas they tend to be non-luminescent in dilute states. This type of luminescence is termed clusterization-triggered emission (CTE), and luminous materials are known as clusteroluminogens. Through-space interactions between polymeric materials, such as hydrogen bonds, ionic interactions, and dipole-dipole interactions, induce through-space conjugations. This leads to extended electron delocalization, which lowers the energy gap and results in emission.[4–10]

Chitosan (CS) is rich in heteroatoms such as N, O, and C=O groups derived from the amide group of chitin. CS is a candidate for CTE owing to the abundant presence of lone-paired electrons of the heteroatoms.[11,12] Among CS-based materials, chitosan nanofibers (CSNFs) are attractive building blocks for functional materials because of their excellent physicochemical stability and dispersibility in aqueous media.[13] Moreover, strong hydrogen bonding and possible ionic

interactions in nanofibrous structures derived from the presence of hydroxyl and amino groups are effective strategies for enhancing CTE properties with stable performance.[11]

Non-conventional luminescence utilizing CTE is challenging for hydrogels because the flexibility of the hydrogel matrix and aqueous conditions may cause cluster disaggregation or non-radiative decay. As stretchable materials, hydrogels with photo-luminous ability are useful in many applications such as bioimaging. To introduce photoluminescence (PL) properties into hydrogels, it is necessary to create luminogens that are less affected by hydration and have a relatively high mobility of the polymer network. Heterogeneous doping of clusters by the compositing method has become an effective way to realize fluorescence in hydrogels because it does not influence the selection of the polymer species that construct the hydrogel network, enabling the tunability of fluorescence. Therefore, it represents a viable route toward the development of photoluminescent clustered fillers with high stability in aqueous environments utilizing biomass resources and their characteristics.[14]

In this study, a clusterofluorophore was fabricated using a combination of CSNFs and dialdehyde carboxymethyl cellulose (DACMC) by a simple synthesis process: mixing a CSNFs suspension with a DACMC aqueous solution, leading to the formation of microparticles. Multiple cross-links of imine bonds, ionic interactions, and hydrogen bonds between the polymers create heteroatomic clusters that exhibit CTE with suitable stability, even in the presence of water. These water-suspended micro-clusters (MCs) were used as CTE fillers in poly(vinyl alcohol) (PVA) hydrogel. The CTE properties of the MCs and composite hydrogels were evaluated based on the concentration of MCs, excitation wavelength, temperature, and solvent. Moreover, metal ions were detected by observing the quenching behavior of the MCs. This work will uncover new strategies for producing CTE materials in an environmentally friendly and efficient manner based on the cross-linking of polysaccharides.

3-2. Experimental Section

Materials and methods

Carboxymethyl cellulose (CMC) was purchased from Sigma-Aldrich (United States), chitosan nanofibers (CSNFs) from Sugino Machine Ltd. (Japan), and hydroxylamine hydrochloride (HAHCl) from Tokyo Chemical Industry Co., Ltd., Japan. Sodium periodate ($NaIO_4$), sodium hydroxide (NaOH), hydrochloric acid (HCl), calcium chloride ($CaCl_2$), magnesium chloride ($MgCl_2$), zinc chloride ($ZnCl_2$), barium chloride ($BaCl_2$), ferric chloride ($FeCl_3$), copper chloride ($CuCl_2$), ammonium chloride (NH_4Cl), ethanol, methanol, and dimethyl sulfoxide (DMSO) were purchased from FUJIFILM Wako Pure Chemical Corporation (Japan). Poly(vinyl alcohol) (PVA) chemical was purchased from the Kishida Company (Japan). All chemicals were used as received.

Synthesis of the CSNFs-DACMC micro-clusters and the PVA-MCs gel composites

An excess amount of 5 wt % DACMC (prepared using the same method that was explained in Chapter 2) aqueous solution was added to a 100 ml aqueous suspension of 1 wt % CSNFs (pH ≈ 6.3). The sample was stirred overnight and allowed to precipitate. Then, the precipitation was cured at 25 °C for 24 h. The sample was purified by washing with deionized (DI) water. Finally, the purified product was sonicated until evenly dispersed.

The evenly dispersed sample was added to a PVA aqueous solution in different weight ratios of 0.5, 1, and 1.5 wt%. The PVA content was maintained at 5 wt% under all conditions. The samples were stirred until they were evenly dispersed; then, the mixtures were molded and FT cycles were carried out. Freezing was done at -25 °C for 10 h and the thawing was done at 4 °C for 2 h. Finally, the gel samples were stabilized in water and stored at 4 °C.

Characterization of the composite

Material characterization was performed using attenuated total reflection-Fourier transform infrared (ATR-FTIR) spectroscopy (Thermo Scientific Nicolet iS5 equipped with an iD5 ATR attachment, United States), with scans conducted over a wavenumber range from 4000 to 500 cm^{-1}. The samples were frozen in liquid nitrogen and lyophilized in a vacuum freeze-dryer. The particle size of MCs was analyzed using a Zeta potential and particle size analyzer (Photal Otsuka

Electronics, Japan). The UV-vis absorbance was measured using a J-820 AC, (JASCO Corporation, Japan). The morphologies of the wet sample were examined under a digital microscope (HiROX HR-5000, USA). The photoluminescence (PL) behaviors of the MCs and hydrogels were examined using a microplate reader (SH-900 Lab, Yamamoto Scientific Co. Ltd., Tokyo, Japan). Additionally, the PL spectra of **Figure. 4b** were taken using JASCO FP-8500 Spectrofluorometer at 360 nm excitation wavelength.

Compression and tensile tests were conducted separately on the hydrogels. For the wet samples, a 10 N load cell was employed. Compression tests were performed at a rate of 3 mm/min, and tensile tests were performed at a rate of 30 mm/min using a universal testing machine (UTM) (Shimadzu EZ Graph, Japan).

3-3. Results and Discussion

The CSNFs-DACMC MCs were developed by simply mixing an aqueous suspension of CSNFs and a DACMC aqueous solution and allowing them to co-assemble to form micro-scale particles, as illustrated in **Figure 1a**. The commercially available CSNFs were produced using the aqueous counter-collision method (**Figure 1c**). The co-assembly of CSNFs and DACMC was facilitated by the formation of imine bonds between the primary amino groups of the CSNFs and the aldehyde moieties of DACMC (**Figure 1b**). The ionic interactions between the amino groups of the CSNFs and the carboxyl groups of DACMC and physical interactions, such as hydrogen bonds between the abundant hydroxyl groups of both polysaccharides, allowed the formation of stable MC precipitates after mixing (**Figure 1d**). The sample was then stirred thoroughly to enhance the reaction, and the mixture was cured at room temperature. Finally, the MCs were dispersed in water by ultra-sonication. Observation of the MCs suspension by the naked eye and photomicroscopy revealed that the size of the coagulated particles was microscale with wide distributions (**Figure 1e**) In contrast to the CSNFs, which were pale yellow, the MCs were dark yellow. This is mainly due to the formation of imine bonds in the MCs.

Fourier transform infrared (FTIR) spectroscopy was performed to characterize the chemical bonding within the materials. For DACMC, a peak at 1590 cm^{-1} corresponding to the C=O stretching vibration of the carboxylate group of CMC was observed. Additionally, a distinct peak at 1730 cm^{-1} was identified as the C=O stretching vibration of the aldehyde group, indicating the

successful oxidation by $NaIO_4$. For the CSNFs, the peak at 1500 cm^{-1} was associated with the N-H bending vibration of the amide group, and that at 1600 cm^{-1} was associated with the C=O stretching of the amide group. Notably, in the FTIR spectra of CSNF-DACMC composites, the intensity of the prominent aldehyde peak of DACMC at 1730 cm^{-1} was significantly decreased, supporting the formation of imine bonds. This observation indicates the cross-linking via imine

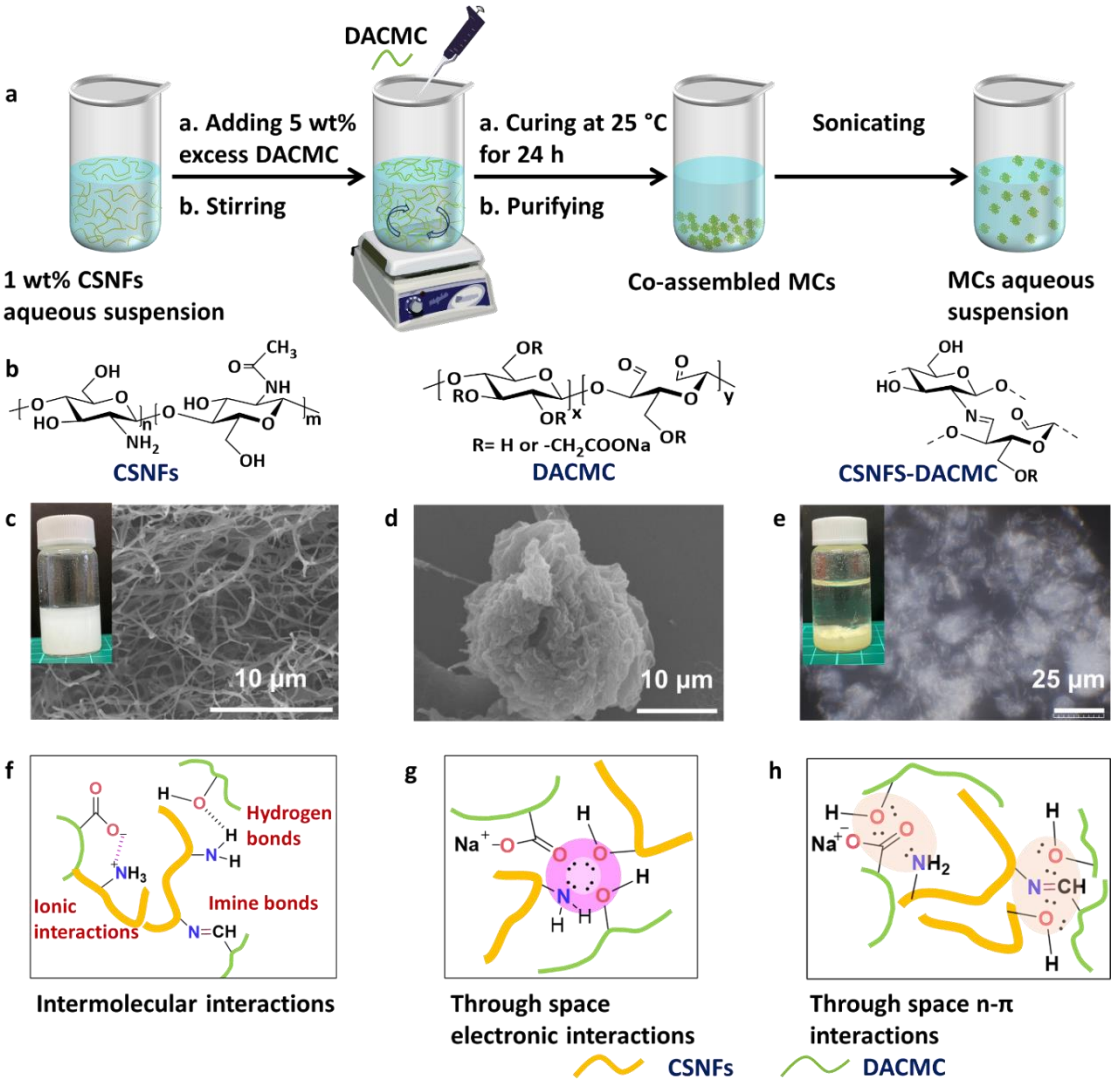

Figure 3-1. (a) Schematic of the fabrication of CSNFs-DACMC MCs. (b) Chemical structures of CSNFs, DACMC, and imine bond formation between CSNFs and DACMC. SEM images of (c) CSNFS, and (d) aggregated MC (e) Digital microscopic image of MCs. Schematic of the (f) intermolecular interactions, (g) through-space electronic interactions, and (h) through space n-π interactions between CSNFs and DACMC in MCs.

bonds between the aldehyde groups in DACMC and the amino groups in the CSNFs within the MCs (**Figure 1f**).

The PL properties of MCs dispersed in an aqueous phase were initially investigated. **Figure 3-2a,** and **b** show that the fluorescence intensity of the MCs suspension increases with the concentration of the suspension. While individual CSNFs and DACMC showed low PL ability, a significant increase in fluorescence intensity was observed in the co-assembled MCs (**Figure 3-2c, and d**). As shown in **Figure 3-1g**, imine bonds and the other intermolecular interactions make the structure of MCs rigid compared to that of CSNFs enabling through space n-n interactions (O···O or O···N) and n-π interactions ((n) O···C=N (π)). This led to a significant enhancement in the PL of the MCs.[14–17] When the DACMC weight ratio increased from 1:1 to 1:3, the fluorescence intensity initially increased and then decreased. This could be due to the self-quenching effect at high concentrations of fluorescent groups (**Figure 3-2e**).[16,18] The MCs exhibited similar fluorescence properties at various combination ratios of CSNFs to DACMC, showing promising stable performance when these polysaccharides were co-assembled. A redshift in the PL spectra was observed when the excitation wavelength was increased from 280 to 460 nm (**Figure 3-2f**).

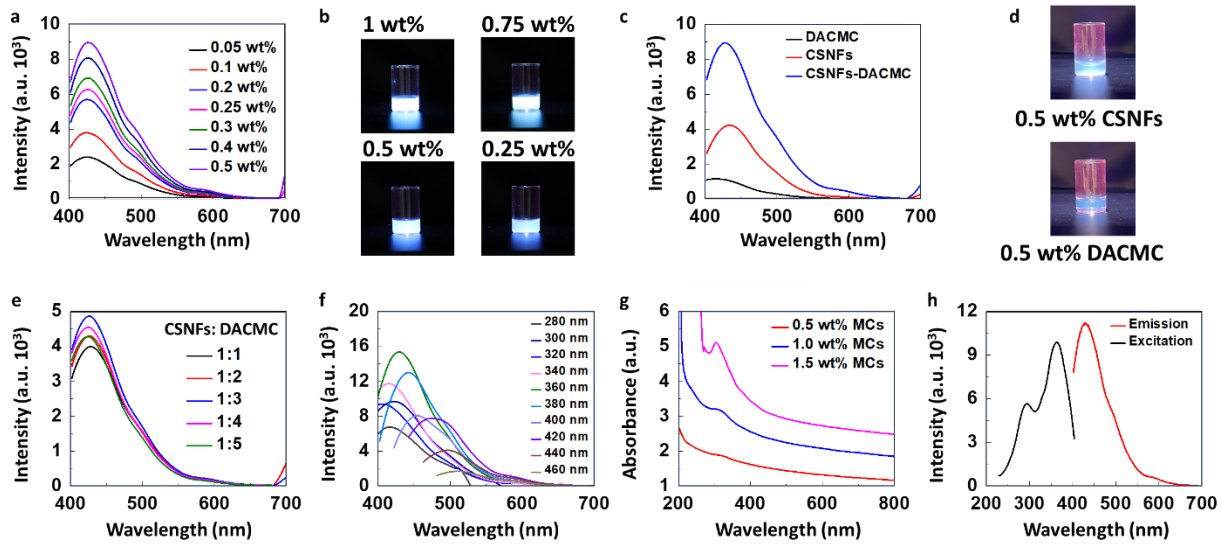

Figure 3-2. (a) PL spectra and (b) photographs of CSNFs-DACMC MCs for different concentrations of MCs (λ_{ex}, 360 nm). Comparison of the (c) PL spectra, and (d) photographs of CSNFs, DACMC, and co-assembled MCs (λ_{ex}, 360 nm). PL spectra of MCs (e) for different weight ratios of added DACMC to the same amount of CSNFs (λ_{ex}, 360 nm), and (f) at different excitation wavelengths. (g) UV-vis absorption spectra of CSNFs-DACMC MCs at different concentrations. (h) Emission and excitation spectra of MCs. (g) Digital microscopic image and photograph of co-assembled CSNFs-DACMC MCs.

This dependence of the luminescence on the excitation wavelength is a general feature of CTE. The widely accepted mechanism is the formation of diverse conformations in clusters with different extents of electron delocalization that are emissive at different energy gaps. This wide distribution of PL centers causes excitation-dependent emission.[7]

The UV-vis absorption spectrum of the MCs showed a peak separation at approximately 320 nm, which may be ascribed to the n→ π * transition of the C=O, and C=N fluorescent groups. Peak separation increased with increasing MCs concentration. The excitation spectrum of the MCs showed that the highest excitation wavelength was 360 nm whereas the highest absorbance wavelength was 305 nm (**Figure 3-2g,** and **h**). The PL stability of the materials was evaluated at different time intervals over 24 h. The PL properties of the MCs were stable for the entire duration. In addition, the MCs exhibited high fluorescence intensities in the dry powder state and as a film. Besides, when CS dissolved in acetic acid aqueous solution was co-assembled with DACMC instead of CSNFs, aggregated precipitations were formed. The aggregates also displayed fluorescence under UV light as well as MCs. However, the aggregates showed low dispersibility even after homogenization by sonication, indicating that CSNFs contributed to the producibility of MCs with good dispersibility in aqueous media. The PL behavior of the MCs was sensitive to temperature changes, showing high intensities at lower

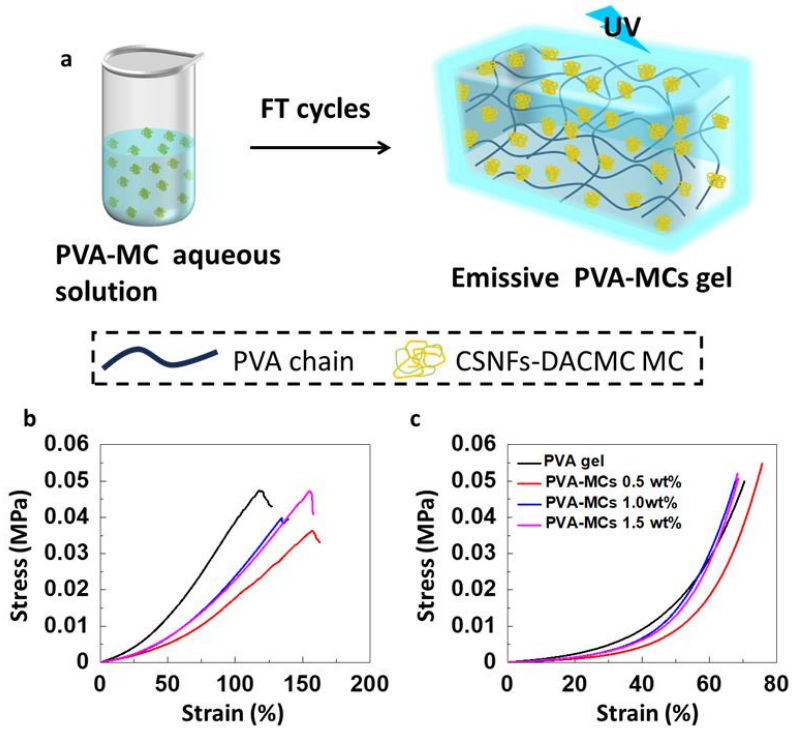

Figure. 3-3. (a) Schematic of the fabrication of the PVA-MCs gel composite and interactions between PVA polymer chains and MCs. (b) Tensile and (c) compression stress-strain spectra of PVA-MCs gels according to the weight % of added MCs.

temperatures (~0 °C) and lower intensities at higher temperatures (~80 °C). This is mainly due to changes in the mobility of molecules; lower mobility under cold conditions might prevent non-radiative decay compared to hot conditions.

The developed MCs were then used to fabricate a hydrogel composite with CTE properties. PVA hydrogel was used as the hydrogel matrix which was formed using the freeze-thaw (FT method, freezing at -25 °C for 10 h and thawing at 4 °C for 2 h.) MCs were added to the PVA solutions, and the mixtures were subjected to three FT cycles to fabricate the PVA-MCs gel (**Figure 3-3a**). The PVA content was maintained at 5 wt%, and the MCs content was varied to 0.5 wt% (PVA-MCs-0.5 wt%), 1 wt% (PVA-MCs-1.0 wt%), and 1.5 wt% (PVA-MCs-1.5 wt%). The PVA-MCs composite hydrogels exhibited stable mechanical properties owing to strong hydrogen bonding among the PVA chains formed during the FT cycles (**Figure 3-3b**, and **c**).

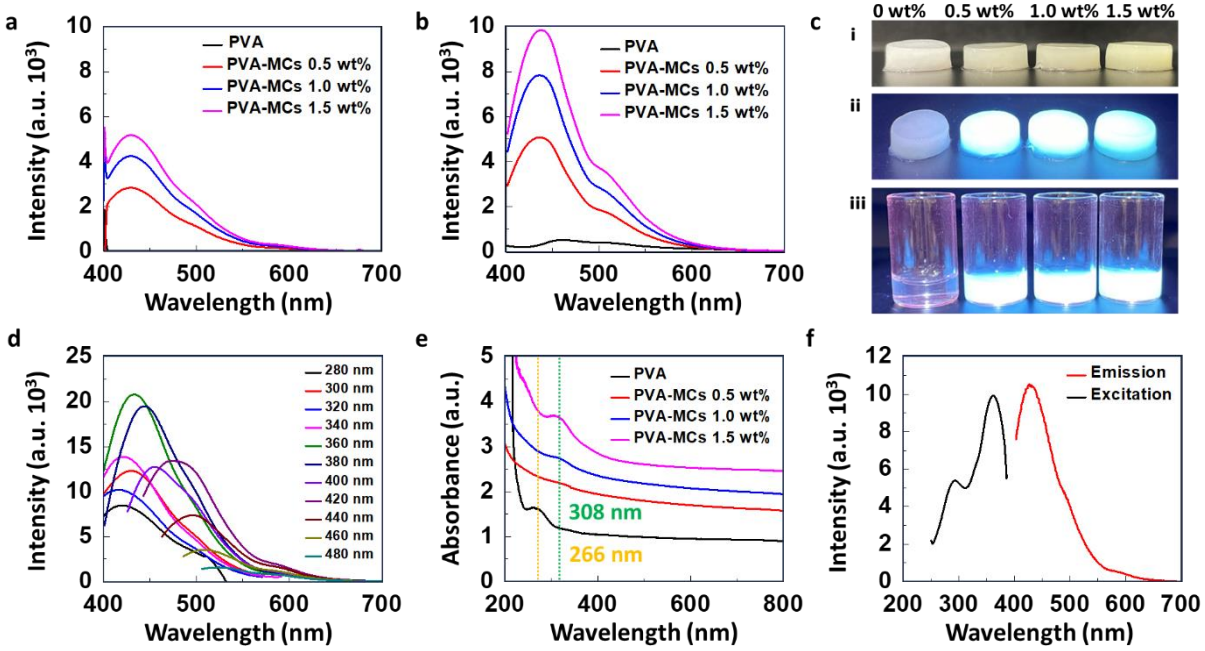

Figure 3-4. PL spectra of PVA-MCs hydrogels (a) before gelation, (b) after gelation (λ_{ex}, 360 nm), and (c) Photographs of the PVA and PVA-MCs hydrogels under i. ambient light, and ii. UV light, and iii. PVA and PVA-MCs gel solutions before gelation under UV light. (d) PL spectra of PVA-MCs hydrogels at different excitation wavelengths. (3) UV-vis absorption spectra of PVA and PVA-MCs gel composites

As shown in **Figure 3-4a, b,** and **c**, both the hydrogel solutions before gelation and the hydrogels exhibited PL. The fluorescence intensity of the hydrogel was significantly higher than that of precursor solutions, suggesting that structural rigidification has a considerable effect after gelation because rigidified clusters minimize the non-radiative relaxations of the excited electrons. In

addition, the abundant hydroxyl groups interacted with the MCs, even though the PVA hydrogel barely exhibited PL. The effect of MCs on the PL properties was confirmed by the preparation of control gel samples by mixing DACMC and CMC aqueous solutions and CSNFs aqueous suspensions. Samples with individual addition of CMC and DACMC showed poor PL, whereas those containing CSNFs showed considerable PL, which was poor compared to the PL of the PVA-MCs composite gels. The hydrogel also exhibited excitation-dependent emission, typically observed in CTE (**Figure 4d**). The UV-vis absorbance spectra of the PVA-MCs gels showed significant peak separation compared to that of the PVA gel. The absorption peak shifted from 266 to 308 nm. Furthermore, the peak intensity increased with increasing MCs content (**Figure 4e**). The relative intensities of the excitation and emission spectra were similar (**Figure 4f**).

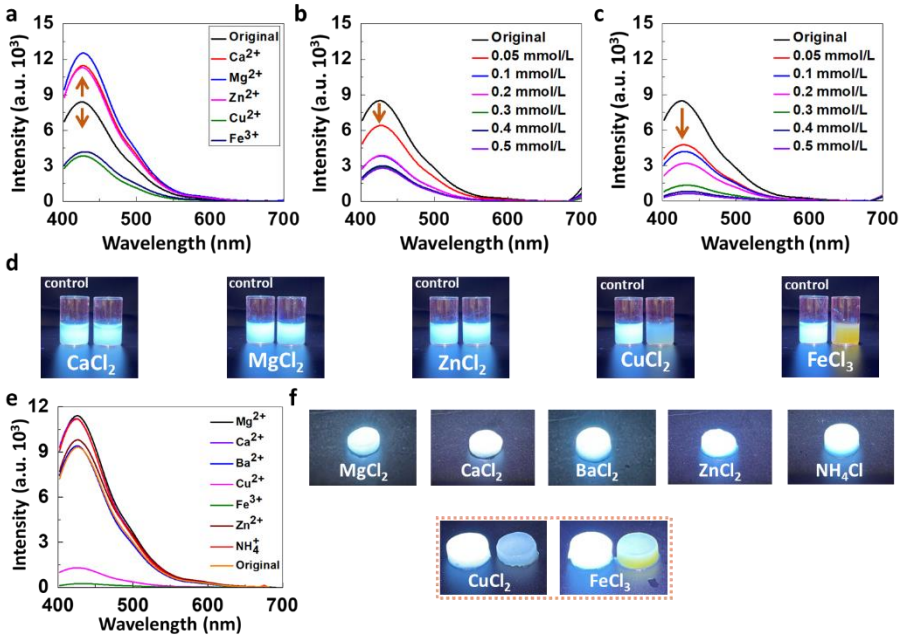

Figure 3-5. (a) PL spectra of MCs aqueous suspension before and after adding 0.1 mmol/L metal chloride solutions. PL spectra of MCs aqueous suspensions added different (b) $CuCl_2$ and (c) $FeCl_3$ solutions. (d) Photographs of MCs aqueous suspensions which added different metal chloride solutions under UV light. (e) PL spectra, and (f) photographs of PVA-MCs hydrogels immersed in different ion chloride solutions under UV light. (λ_{ex}, 360 nm)

Furthermore, the effects of metal ions on the PL of aqueous MCs solutions and hydrogel, and of solvents on that of hydrogels were investigated using various metal chloride salts. Ca^{2+}, Mg^{2+}, and Zn^{2+} ions enhanced the fluorescence intensity of the MCs suspensions and hydrogels. This was

mainly due to the formation of metal clusters of the MCs with these metal ions, which enhanced the conformational restrictions. In particular, the carboxylate groups of DACMC can form metal clusters via electrostatic interactions with these metal ions.[19] In contrast, in both the MC suspensions and hydrogels, there was a quenching of fluorescence in the presence of Fe^{3+} and Cu^{2+} ion solutions (**Figure 3-5a-f**). The relationship between the concentration of these metal ions and fluorescence intensity showed that a strong decreasing trend in intensity was prominently observed in the concentration region below 0.1 mmol/L. Compared to Zn^{2+} ions, these two metal ions have empty d orbitals, which can create additional relaxation pathways for excited electrons.[20,21]

On the other hand, it was found that Fe^{3+} ion solutions can absorb UV in the range of 200-400 nm, which affects the fluorescence of the materials after adding the metal ion solution. However, Cu^{2+} ion solutions did not show absorbance in that range which can show fluorescence quenching due to the abovementioned special reasons. The chloride salt of each metal ion was used because it was observed that the iodide ion is also a PL quencher because of its heavy atom effect. In addition, the fluorescence intensity of the hydrogels immersed in different pH solutions at 4, 7, and 10 was evaluated. The fluorescence intensity was the highest at pH 7, and a slight decrease in the intensity was observed at pH 4 and 10. This supports that the MCs maintain stability and PL performance under various pH conditions. Moreover, the changes in pH did not significantly affect the mechanical strength.

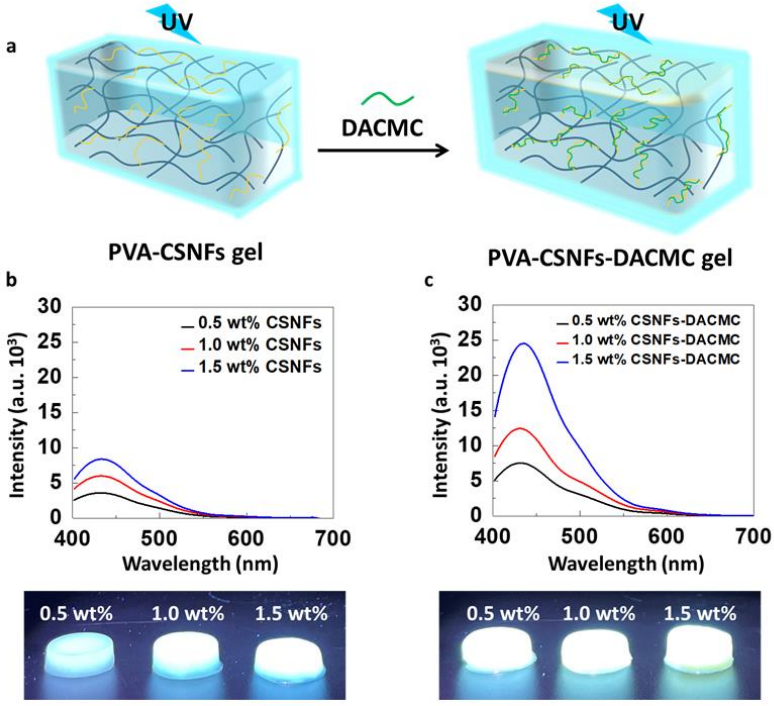

Figure 3-6 (a) Schematic of the preparation of PVA-CSNFs and PVA-CSNFs-DACMC hydrogel. (b) PL spectra and photographs of the PVA-CSNFs hydrogels under UV (λ_{ex}, 360 nm). (c) PL spectra and photographs of PVA-CSNFs-DACMC hydrogels under UV (λ_{ex}, 360 nm).

Finally, a CTE hydrogel was prepared using a post-cross-linking method between the CSNFs and DACMC. In-brief, PVA-CSNFs composite hydrogels were prepared by adding different weight ratios of CSNFs (0.5, 1, and 1.5 wt%) to 5 wt% PVA aqueous solutions (**Figure 3-6**). Subsequently, FT cycles were performed for gelation. Then the hydrogels were immersed in 2.5 wt% DACMC aqueous solutions for 24 h. at 25 °C to fabricate PVA-CSNFs-DACMC hydrogels. A characteristic color change from white to brownish-yellow was observed owing to the incorporation of DACMC into the hydrogel network via multiple bond formations, as was observed for the MCs. The emission intensity of the PVA-CSNFs-DACMC hydrogels was dramatically enhanced compared to PVA-MCs. This is probably due to the pre-immobilization of CSNFs into PVA networks enabled to preserve the dispersibility of CSNFs in the cross-linking process, contributing to a homogeneous distribution of co-assemblies of CSNFs-DACMC in the composite hydrogels. These results indicate that the size and distribution of the co-assembled structure affect the PL properties.

3-4. Conclusions

Photoluminescent MCs were fabricated by the co-assembly of CSNFs and DACMC in aqueous solutions. The MCs were stable in an aqueous environment because of the multiple interactions between them, such as imine bonds, ionic interactions, and hydrogen bonds. Aqueous suspensions of the MCs showed significant PL behavior at λ_{ex} = 360 nm, compared to the control solutions of CSNFs and DACMC due to the rigid cluster formation resulting from the co-assembly. The predicted CTE mechanism is based on the TBC in rigid clusters. MCs were used as fillers to fabricate the PVA-MCs composite hydrogel without disturbing the hydrogel stability in water or its mechanical strength. The composite hydrogel exhibited remarkable emissive properties and stable performance over long periods at various temperatures. In addition, both the MCs and PVA-MCs gels displayed detectability toward metal ions. Ca^{2+}, Mg^{2+}, and Zn^{2+} ions enhanced the fluorescence intensity whereas Fe^{3+} and Cu^{2+} ions significantly quenched the PL of the materials. This behavior of the PVA-MCs gel makes it a promising material for use in metal sensing and bioimaging.

3-5. References

(1) H. Zhang, Z. Zhao, P. R. McGonigal, R. Ye, S. Liu, J. W. Y. Lam, R. T. K. Kwok, W.Z.Yuan, J. Xie, A. L. Rogach, B. Z. Tang, *Mater. Today* **2020**, *32*, 275.

(2) J. Tavakoli, A. J. Ghahfarokhi, Y. Tang, *Curr. Chem. (Chem)* **2021**, *379*, 9.

(3) S. Zhu, Y. Song, J. Shao, X. Zhao, B. Yang, *Angew. Chem*. **2015**, *127*, 14834.

(4) R. Bresolí-Obach, J. A. Castro-Osma, S. Nonell, A. Lara-Sánchez, C. Martín, *JPPC* **2024**, *58*, 100653.

(5) D. Wang, J. Ju, S. Wang, Y. Tan, *J. Mater. Sci. Technol*. **2021**, *76*, 60.

(6) P. Liao, J. Huang, Y. Yan, B. Z. Tang, *Mater. Chem. Front.* **2021**, *5*, 6693.

(7) H. Zhang, B. Z. Tang, *JACS Au*. **2021**, *1*, 1805.

(8) P. Liao, S. Zang, T. Wu, H. Jin, W. Wang, J. Huang, B. Z. Tang, Y. Yan, *Nat. Commun*. **2021**, *12*, 5496.

(9) M. Li, X. Li, X. An, Z. Chen, H. Xiao, *Front. Chem*. **2019**, *7*, 447.

(10) M. A. Johns, A. E. Lewandowska, E. Green, *S. J. Eichhorn. Analyst.* **2020**, *145*, 4836.

(11) D. I. Sánchez-Machado, J. López-Cervantes, M. A. Correa-Murrieta, R. G. Sánchez-Duarte, P. Cruz-Flores, G. S. Ia Mora-Lopez, Nonvitamin and Nonmineral Nutritional Supplements, Elsevier, **2018**, 485.

(12) F. L. Mi, *Biomacromolecules*. **2005**, *6*, 975.

(13) L. Xu, Q. Meng, Z. Zhang, S. Zhong, Y. Gao, X. Cui, *Int. J. Biol. Macromol*. **2022**, *209*, 1124.

(14) H. Ju, H. Zhang, L. X. Hou, M. Zuo, M. Du, F. Huang, Q. Zheng, Z. L. Wu. *J. Am. Chem. Soc*. **2023**, *145*, 3763.

(15) W. Wang, M. Liu, W. Gao, Y. Sun, X. Dong, *ACS Appl. Mater. Interfaces* **2021**, *13*, 55879.

(16) Q. Li, X. Wang, Q. Huang, Z. Li, B. Z. Tang, S. Mao, *Nat. Commun*. **2023**, *14*, 409.

(17) X. Dou, Q. Zhou, X. Chen, Y. Tan, X. He, P. Lu, K. Sui, B. Z. Tang, Y. Zhang, W. Z. Yuan *Biomacromolecules* **2018***, 19,* 2014.

(18) J. Song, H. Zhou, R. Gao, Y. Zhang, H. Zhang, Y. Zhang, G. Wang, P. K. Wong, H. Zhao. ACS Sens. 2018, 3, 792.

(19) J. Huang, Y. L. Wang, X. D. Yu, Y. N. Zhou, L. Q. Chu, *Int. J. Biol. Macromol.* **2020**, *152*, 50.

(20) X. Jiang, Q. Wang, B. Li, S. Li, X. Z. Kong, *J. Polym. Sci. (Engl. Ed.)* **2023**, *41*, 129.

(21) D. Tong, W. Li, Y. Zhao, L. Zhang, J. Zheng, T. Cai, S. Liu, *RSC Adv*. **2016**, *6*, 97137.

Conclusion Remarks

In this doctoral thesis, composite materials based on chitosan (CS) and cellulose with cross-linked networks were successfully fabricated, demonstrating multiple characteristics for various applications depending on their structural forms. The structural and chemical diversity of both chitosan and cellulose was leveraged to create three different composite materials using various methods with multiple cross-linking.

In Chapter 1, stimuli-responsive all-polysaccharide composites were successfully prepared by combining cellulose nanofibers (CNFs) and chitosan (CS). Bacterial cellulose (BC), a natural hydrogel with tightly packed cellulose nanofibers (CNFs) was oxidized into dialdehyde BC (DABC) and was composited with chitosan (CS), a readily available natural polymer, to develop a mechanically adaptive hydrogel composite under different pH conditions. Composites exhibit pH sensitivity by presenting higher mechanical properties under acidic conditions and lower mechanical properties under basic conditions owing to the protonation of amino groups of the chitosan chains. Osmotic pressure is built up under acidic conditions, increasing the mechanical strength of the composites. The good three-dimensional stability of composites enables them to consistently maintain their volume when exposed to acidic or basic conditions. This research addressed the limitation in applying pH-responsive hydrogels due to their concomitant swelling and shrinking.

In Chapter 2, sponge materials comprising biomass resources, specifically CSNFs and DACMC, were successfully synthesized using a freeze-thaw method complemented by post-cross-linking during the thawing phase. The fabrication of porous sponge materials with stable structures via crosslinking diverse polymers presents significant challenges due to the simultaneous requirements for phase separation as a pore-forming step and cross-linking reactions during the fabrication process. This novel approach utilized ice crystals as a template for pore formation during the freezing steps of the CSNFs media, leading to the concentration of the CSNF-rich phase. Subsequent thawing facilitated the gradual diffusion of DACMC from the thawed CSNFs medium, enabling the formation of stable porous structures through ionic interactions and imine bonds. The resulting cross-linked structure enhanced the mechanical stability of the sponge and its overall porous integrity. employing a straightforward, eco-friendly technique. This method effectively

addresses the difficulties associated with pore formation in materials, which typically arise from the rapid formation and precipitation of polyionic complexes during the mixing of anionic and cationic polymers, using ice crystals as a rigid template. The resultant sponge materials exhibit remarkable shape recoverability in their wet state and maintain light, stable porosity in the dry state. Furthermore, in comparison to commonly used commercial foams, this composite porous material demonstrates superior fire retardancy and thermal insulation properties in its dry state. Additionally, it shows effective adsorption capacities for both cationic and anionic dyes and metal ions. This method of using bio-based polymers to produce porous composites offers a promising avenue for creating multifunctional materials, with potential applications across various industries.

In Chapter 3, co-assembled micro-clusters (MCs) were fabricated using chitosan nanofibers (CSNFs) crosslinked with dialdehyde carboxymethyl cellulose (DACMC). MCs form stable structures under aqueous conditions owing to the formation of cross-links via imine bonds, ionic interactions, and hydrogen bonds between the polysaccharides. These multiple interactions and the heteroatomic nature of both CSNFs and DACMC enable the realization of clusterization-triggered emission (CTE) by through-space conjugation. MCs exhibit stable fluorescence behavior under aqueous conditions. A composite gel of MCs and poly (vinyl alcohol) (PVA) (PVA-MCs) was synthesized using the freeze-thaw method to develop CTE hydrogel. The MCs and PVA-MCs gels demonstrated the detection ability toward specific metal ions such as Cu^{2+} and Fe^{3+}, by the quenching of the emission. This strategy for the creation of CTE MCs based on cross-linked polysaccharides widens the scope of the practical and sustainable application of water-containing fluorescent materials in the fields of sensing and biomedicines.

In conclusion, the author developed strategies to construct polysaccharide-based materials utilizing cross-links as key structures. The strategic use of cross-linking and multiple interactions was crucial in achieving these functionalities. This approach realized various functions, widening the scope of practical and sustainable applications, thereby enhancing the environmental benefits of using sustainable resources in material engineering.

List of Publications

1. Stimuli-responsive composite hydrogels with three-dimensional stability prepared using oxidized cellulose nanofibers and chitosan

Madhurangika Panchabashini Horathal Pedige, Taka-Aki Asoh, Yu-I Hsu, Hiroshi Uyama

Carbohydrate Polymers, **2021**, *278,* 118907.

DOI: 10.1016/j.carbpol.2021.118907

2. Multifunctional Chitosan Nanofiber-Based Sponge Materials Using Freeze-Thaw and Post-Cross-Linking Method

Madhurangika Panchabashini Horathal Pedige, Akihide Sugawara, Hiroshi Uyama

ACS Omega, **2024,** *9,* 36464.

DOI: 10.1021/acsomega.4c04317

3. Clusterization-triggered emission of polysaccharide-based microclusters induced by co-assembly of chitosan nanofibers and dialdehyde carboxymethyl cellulose

Madhurangika Panchabashini Horathal Pedige, Akihide Sugawara, Hiroshi Uyama

Bulletin of the Chemical Society of Japan, **2024**, *97*.

DOI: 10.1093/bulcsj/uoae065

Acknowledgments

This study, presented in this thesis, was conducted at the Department of Chemistry, Graduate School of Engineering, Osaka University, from 2019 to 2024. The journey was filled with numerous experiences that shaped who I am today. This achievement was made possible by the great opportunities I encountered and the amazing people I met along the way.

I am deeply grateful to Osaka University and the Japanese Ministry of Education, Culture, Sports, Science and Technology (MEXT) for providing me with the opportunity to pursue my graduate studies at Osaka University. I sincerely appreciate the financial support from MEXT over the past five years, which has been instrumental in my academic journey.

I would like to express my sincere gratitude to my supervisor, Professor Hiroshi Uyama of Osaka University, for his unwavering belief in me and for the invaluable experience of working in the Uyama laboratory as a master student from 2019 to 2021 and a doctoral student from 2021 to 2024. His encouragement and the numerous opportunities he provided have been crucial in my development as a researcher. I would also like to thank the rest of my thesis committee: Prof. Takashi Hayashi and Prof. Masaya Nogi for their insightful comments, as well as their generous contribution of time to the preparation of this thesis.

I would like to convey my heartfelt gratitude to Assoc. Prof. Taka-Aki Asoh (currently appointed at Tokyo University of Science) served as my advisor during my initial research projects and imparted essential skills to me. I also extend my sincere thanks to Assist. Prof. Akihide Sugawara for his invaluable assistance with my research work, the preparation of my thesis and manuscripts, as well as his insightful comments and recommendations. Additionally, I extend my special thanks to Assoc. Professor Yu-I Hsu for her encouragement and suggestions whenever I encountered obstacles.

I am also grateful to Prof. Norimitsu Tohnai and Assist. Prof. Shotaro Nakamura for their valuable support in the validation of my third research work.

I would like to extend my heartfelt gratitude to Ms.Yoko Uenishi, and Ms.Tomoko Shimizu for their kindness for these five years. Also, Ms. Kyoko Tanimura, Ms. Erina Katsuragawa, Ms. Chikako Abe, Ms. Rieko Yagi, Ms. Yasuko Matsuda, and Ms Kyoko Fuma for their support and the friendly environment.

I would like to express my deepest gratitude to all the members who worked in the Uyama Laboratory between 2019 and 2024 for their wholehearted support and kind assistance in both research and daily life. I would like to extend a special thank you to Lec. Prof. Chen Qian (School of Material Science and

Engineering, Zhejian Sci-Tech University) for his valuable guidance in the research works in my first year of the master's program. Also I am very thankful to Dr. Toshiki Tamiya, Dr. Shunsuke Mizuno, Dr. Bozhi Chen, Dr. Naharullah Bin Jamaluddin, Dr. Yankun Jia, Dr. Raghav Soni, Dr. Hanyu Wen, Dr. Yanting Lyu, Dr. Yan Wang, Dr. Luwei Zhang, Dr. Meng Wei, Dr. Mark Adam Malaluan Ferry, Dr. Yuxiang Jia, Dr. Nontarin Roopsung, Mr. Toshiki Honda, Mr. Yuya Fujiwara, Mr. Ginga Hoshi, Mr. Tatsuya Yamamoto, Mr. Emil Hajili, Ms. Manjie He, Mr. Yu Cao, Mr. Peng Du, Ms. Juan Wang, Mr. Kazuki Shibasaki, Mr. Atsuki Takagi, Ms. May Myat Noe, Ms. Hasinah Binti Mohamed Rafiq, Ms. Judit Rebeka Molnár, Ms. Guan Wang, Ms.Ying Yao, Mr. Ruiqi Zhang, Mr. Yihan Gao, Mr. Kohei Kikkawa, Ms. Airi Ozaki, Ms. Jiaxin Alice Chen, Ms. Zeying Cao, Ms. Linxuan Li, Ms. Yuka Kashihara, Ms. Shiho Takai, Mr. Yuji Kiba, Mr. Takeshi Hiraoka, Mr. Yuki Shioji, Mr. Atsushi Koizumi, Mr. Motoi Oda, Mr. Kaita Kikuchi, Mr. Koki Tsujita, Mr. Hajime Fujimori, Ms. Suzune Miki, Ms. Thuy Le Huynh An, Ms. Izzah Durrati Binti Haji Abdul, Ms. Sooyeon Noh, Mr. Xinyu Lou, Mr. Hiroshi Hasegawa, Mr. Shotaro Yano, Mr. Kippei Yamamura, Ms. Rika Onishi, Ms. Hajah Wafiqah Binti Haji Daim, Ms. Ziyu Meng Ms. Shafinee Yarnina Hj Md Shafri, Mr. Alejandro Adrian Ayala Escamilla, Ms. Daniela Yacine Sebastião Bravo Da Costa, Mr. Jiahui Dong, Ms. Yuka Asai, Mr. Yinxiang Shen, Ms. Moe Kominami, Ms. Akane Odagaki, Ms. Rina Kugimiya, Mr. Shunya Kubo, Mr. Sota Nakagawa, Ms. Maoko Hayashi, Mr. Shunsuke Kondo, Mr. Yudai Ioku, Mr. Naoaki Ishihara, Mr. Yuta Okuda, Ms. Kanoko Sakai, and Mr. Takehiro Masuda.

I am grateful for the support I have received from both local and distant friends, including, Ms. Kaori Takahashi, Ms. Sakiyo Nakama, Ms. Pavani, Ms. Dakshika, Ms. Chalani, Ms. Shashini, Ms. Kithma, Ms.Wathsala, Mr. Dhananjaya, Mr. Sandakelum, and Ms. Butsaratip Suwattananurak. Their support has been invaluable to me throughout this journey.

Lastly, I would like to express my heartfelt appreciation to my parents, Vilbet, and Rajeshvaree, my parents-in-law Indrawansha, and Siriyawathie, my sisters Jeewani, Kalpani, Indunil, and Sandakelum, my brothers Lakmal, Rangana, Sandeep, Amila, and Manula for their thoughtful attention and continuous encouragement. Finally, I am deeply grateful to my husband Nuwan, who was always there for me, providing unwavering affection and care. Your constant support, encouragement, and love have been my strength throughout this journey. Thank you for standing by my side and being my rock.

June 2024.

H. P. M. Panchabashini